NSG - 7172

N78-13076

UNIVERSITY OF SOUTHAMPTON

department of aeronautics and astronautics

Self Streamlining Wind Tunnel - Low Speed Testing and Transonic Test Section Design

Semi-annual Progress Report

April 1976 - December 1976

(NASA-CR-145257) SELF STREAMLINING WIND TUNNEL: LOW SPEED TESTING AND TRANSONIC TEST SECTION DESIGN Semiannual Progress Report, Apr. 1976 - Dec. 1976 (Southampton Univ.) 70 p HC A04/MF A01 CSCL 14B G3/09

N78-13076

Unclas
55126

SELF STREAMLINING WIND TUNNEL - LOW SPEED TESTING AND TRANSONIC TEST SECTION DESIGN

by

S.W.D. Wolf
M.J. Goodyer
Department of Aeronautics and Astronautics
The University
Southampton, U.K.

This is a semi-annual Progress Report, April 1976 - December 1976, on work undertaken on NASA Grant NSG-7172 entitled "The Self Streamlining of the Test Section of a Transonic Wind Tunnel". The Principal Investigator is Dr. M.J. Goodyer.

CONTENTS

CONTENTS

1. INTRODUCTION

The objective of work carried out with the low speed Self-Streamlining Wind Tunnel (SSWT) at Southampton University has been to gather aerodynamic data on an airfoil section for comparison with other results obtained on the same section in a conventional wind tunnel, to show the reduction of wall interference with streamlining. The previously published experimental results from the SSWT have been very limited, namely pressure distributions around a cylinder and around a NACA 0012-64 airfoil at 6^{o} angle of attack[1]. The main reason for the paucity of data was that around eight iterative steps were required to streamline the flexible walls per test, and each step required a protracted involvement with tunnel and computer. A predictive method for rapid wall adjustment has now been devised, allowing an increase in the rate of testing. This report includes fairly comprehensive data on the airfoil through a wide range of angle of attack, both stalled and unstalled.

Analysis of aspects of the design of flexible walled test sections has continued, with immediate application to the design of the new transonic test section. It is shown that the magnitude of the deviation of the contour of a wall from the shape of a streamline, arising from inevitable errors in wall position estimation and from the fact of having control over the position at only a finite number of points, is probably acceptable in terms of the effect of such errors on the aerodynamic behaviour of a model.

The design of the transonic test section is outlined, drawing on these and earlier analyses[1], for eventual coupling to a digital computer for the automatic contouring of the walls.

2. LOW SPEED SELF-STREAMLINING WIND TUNNEL EXPERIMENTAL RESULTS

During the latest series of tests, the SSWT has remained largely unaltered in design since the last Progress Report[1], and is operating with a test section depth-to-chord ratio of approximately unity ($h/c \doteq 1$). However, to introduce more symmetry into the geometry of the test section there has been an addition of two extra jacks and a length of straight wall to the downstream end of each flexible wall. There are no pressure tappings at these new jacks. This change has moved the open jet of the test section a further 22.9cm. (9 inches) downstream, and should have the effect of reducing the interference effects of the truncation of the length of the test section[1]. A new jack with pressure tapping and rib has also been positioned on each wall roughly in line with the wing leading edge.

The NACA 0012-64 airfoil was tested in various conditions, initially with only leading edge transition strips, but later with the addition of trailing edge or leading edge fences. The airfoil has a chord of 13.72cm. (5.4 inches), with thirty-nine chordwise distributed pressure tappings on its surface. For comparative purposes the identical model has been tested in the 7 foot by 3 foot test section of the Low Turbulence Pressure Tunnel (LTPT) at NASA Langley Research Center, where aerodynamic data was obtained relatively free from tunnel interference, with a test section depth to wing chord ratio (h/c) of 16.7.

The series of SSWT tests covered airfoil angles of attack from -6° to $+12^{\circ}$, with the Mach number at approximately 0.1 throughout. Although the new wall setting strategy reduced the number of iteration steps to obtain streamlined walls (as will be shown later), as the SSWT is still adjusted manually the time required for setting up the wind tunnel for each run remains inconveniently long, of order 3 hours.

The series of runs is summarised by the table in Figure 2.1, which shows that most of the 15 tests involved iterations. Each test was terminated when the flexible-walls were deemed to be streamlined and data had been taken from the airfoil. All of the aerodynamic data obtained on the wing following the wall streamlining process is shown in Figure 2.2, and may be compared directly with the LTPT results. For clarity the latter are shown as lines, although they were in fact point measurements. It can clearly be seen from these graphs that the SSWT and LTPT data agree well when the airfoil is unstalled (α less than about 8°). But conversely they illustrate a rather slow drop in the airfoil suction pressures in the SSWT as the angle of attack progresses beyond stall, which has resulted in the airfoil producing a higher lift coefficient than during the corresponding LTPT test.

The behaviour of the airfoil is summarised by the variations of the normal force coefficient C_N and the chordwise force coefficient C_C with angle of attack. These coefficients are defined in Figure 2.3.

The C_N - α data is shown on Figure 2.4(a) below stall and on Figure 2.4(b) for angles of attack through stall. The C_C - α data is on Figure 2.5.

The slope of the C_N - α curve for the SSWT data is in good agreement with that from LTPT below stall. On Figure 2.4(a) straight lines are drawn through the two sets of data using the least squares method. In the range $-6^o < \alpha < 7^o$ the slopes of the lines and their $C_N = 0$ intercepts are:

Tunnel	$\partial C_N / \partial \alpha$ (per degree)	Zero C_N Intercept
LTPT	0.08595	$-.121^o$
SSWT	0.08372	$+.228^o$

The ratio of SSWT to LTPT C_N - α slopes is 0.974.

At values of α above 8^o differences between the two slopes become significant. The LTPT curve has a relatively sharp peak at $\alpha = +9^o$, beyond which the slope becomes steeply negative, whereas the SSWT data shows a more gradual rise to a slightly lower maximum, occurring in the region of $\alpha = 11^o$, followed by a more gradual fall in C_N.

The C_C - α plot on Figure 2.5 again shows good agreement between the two sets of data except for an apparent shift in the SSWT data towards more positive angles of attack, in most regions the shift is about half a degree, roughly in agreement with an equivalent shift in the C_N - α data.

A trailing edge stall was expected for this airfoil, and it was thought that complete separation may not have been occurring in the SSWT tests. One possible reason for this was secondary flows, and it was therefore decided to try some simple 'aerodynamic fixes' on the airfoil.

Firstly, two disc shaped leading edge fences were fitted to the model 1.2cm. (half an inch) from the sidewalls, for test 13 at $\alpha = 12^{o}$. The results plotted in Figures 2.4 and 2.5 for this test show that the normal force was reduced, but the discrepancies between SSWT and LTPT C_N and C_C values were only halved in the stalled regime. Further tests at $\alpha = +6^{o}$ and $+9^{o}$ yielded little change in C_N and C_C. Surface flow visualisation was used in these tests to check that the flow around the airfoil was two dimensional. A fluourescent dye was deposited in discrete spots on the wing surface and photographed in ultra violet light after a brief run of the tunnel. Some photographs are reproduced in Figure 2.6. It will be noticed that in the SSWT for $\alpha = +12^{o}$, the airfoil is in fact set 12^{o} nosedown since the airfoil is mounted upside-down. The flow over the pressure surface appears to be two dimensional even near the wing fences, while the suction surface displays a more irregular and confused pattern, with leading edge separation and a large region of reverse flow. The dye trails have a definite tendency towards one side of the wind tunnel, indicating the existence of some three dimensional effect. The dye on one of the wing fences shows that there is only a small separation bubble on the wing leading edge.

A possible explanation for the asymmetry of the suction surface flow could have been the random nature of the grit concentrations on the leading edge of the airfoil. The same method of attaching the grit to the model had been employed both at Langley and Southampton to ensure similar grit distributions, but over a period of time some grit may have become detached from the airfoil. It was therefore re-gritted with the same size of grit, but in larger quantities and in approximately constant concentrations spanwise. The test that followed showed that the suction surface flow pattern had indeed been affected. The diagram in Figure 2.7 compares the surface flow patterns with the two grit concentrations and shows that with extra grit the flow over the suction surface is more nearly two dimensional. However, no significant change in airfoil pressure data was noted during the test, and the problem with stall data has remained unresolved.

To this point the open jet at the downstream end of the test section had remained fixed in position. That is, the two new jacks furthest downstream on each wall had not been moved once the walls had been set straight with an empty test section. There was therefore the possibility that as the flow area at the downstream end of the test section was being maintained constant, the wake from the stalled airfoil was being constrained too much, with an effect being fed upstream.

However, test 14 which was carried out with the leading edge fences in place at $+12^{\circ}$ angle of attack, but

with the downstream ends of the flexible walls moved out a distance given by the wall setting strategy, when the real-side pressure coefficients were assumed the same as for jack 16 at the new jacks 17 and 18. This change brought about no significant effects at the wing, despite relatively large movements of the open jet and an overall increase in flow area. Figure 2.8 shows how the geometry of the open jet altered between Tests 13 and 14.

The final aerodynamic fix was the addition to the wing of trailing edge fences 1.2cm. (half an inch) from the sidewalls. When tested with the trailing edge fences alone it was found after re-streamlining the walls that the airfoil pressure distribution at 12^{o} angle of attack had changed significantly, but in the wrong direction. The distributions with trailing edge fences, and with leading edge fences, are shown on Figure 2.9, while surface flow details are shown on Figure 2.10.

No explanation for the differences between LTPT and SSWT data at high angles of attack can be offered at the time of writing.

Some of the streamlined contours which the flexible walls adopted during these tests are presented as an aid to future designs of test sections. All jack position measurements were made relative to a datum, which in this case is the set of positions giving the "straight wall" contours. The streamline contours with $\alpha = +6^{o}$ and $+12^{o}$ are shown on Figure 2.11. The maximum deflections from straight shown on this Figure represent about the maxima

expected with this combination of airfoil and test section.

While attempts made so far to reduce the discrepancies between the two sources of airfoil data at high angles of attack have failed, efforts to close the gap continue. There are many possible reasons for discrepancy. One might be a sensitivity of stall to free stream turbulence. Although no measurements have been made of the turbulence level in the SSWT, it is most probably higher than in LTPT with the attendant possibility of the effective Reynolds number in SSWT being higher than in LTPT. Data taken in LTPT on this airfoil over a range of Reynolds numbers has shown at some angles of attack and at certain stations on the airfoil an extreme sensitivity to Reynolds number.

The wall setting strategy is outlined in the following section. There is a possibility of some characteristic of this method introducing errors when the flow is separated from the model, while giving good data with attached flow. Both of these possibilities are currently receiving attention.

3. WALL SETTING STRATEGY

The wall setting strategy for rapid wall adjustment which was described in Reference 1 has now been adapted for use with the low speed SSWT. The basis remains unaltered, but there have been certain detailed changes.

The earliest method of wall adjustment[2] utilised the error between the real and imaginary pressures to determine wall movements. While there was no doubt about the necessary direction of movements, suitable magnitudes were determined only by experience.

The new method predicts analytically the required movement, offering the possibility of reducing the number of iteration steps in the streamlining process from approximately eight which had been necessary to move from straight walls to streamlines, prior to its introduction.

The wall setting strategy was based originally on an analytical model which consisted of a single flexible-wall adjacent to an arbitrary wind tunnel model. An iterative process resulted from the fact that the flow around the model is modified by each wall movement. However, no account was taken of the effect of interactions between the two flexible walls, and this proved to be a serious omission.

The first SSWT tests using the wall setting strategy proved that it was in fact unstable, the walls gradually moving further and further apart with each step. An analytical link was required between the two flexible walls to reduce the effects of the aerodynamic coupling and to

speed up the wall streamlining. The coupling was introduced by means of scaling factors a_1 and a_2 in the forms

$$Y_B = y_B + a_1 \cdot y_T$$
$$Y_T = y_T + a_2 \cdot y_B \qquad 2.1$$

where Y_B, Y_T are local wall movements (away from the model) required on the top and bottom walls respectively before the next test, and y_B and y_T are the required movements for bottom and top walls respectively calculated by the original[1] method. The choice of values for a_1 and a_2 affected the stability of the wall adjustment, but satisfactory behaviour was obtained with each set at 0.35.

In this form it was demonstrated in early tests that the flexible walls could be adjusted from straight to streamlined contours typically in four iterations, and if a new angle of attack was set within about 2^o of the old angle the new streamlined contours could often be selected in just one step from the old streamlined contours.

However, it was noticed in most tests that the first wall adjustments usually overshot the eventual streamlined positions of the flexible walls. This effect was reduced by introducing another two factors a_3 and a_4 to scale down the wall movements Y_T and Y_B, in the form below giving new movements Y'_B and Y'_T:

$$Y'_B = a_4 \cdot Y_B + a_1 \cdot a_3 \cdot y_T$$
$$\text{and} \qquad Y'_T = a_3 \cdot y_T + a_2 \cdot a_4 \cdot y_B \qquad 2.2$$

for the bottom and top walls respectively.

Tests 4, 5 and 8 to 14 summarised in Figure 2.1 were made with $a_3 = a_4 = 0.8$, and it can be seen that an average of three iterations was required for these tests all of which started from straight wall contours. The evidence indicates that setting the walls according to equations 2.2 reduces the number of iterations by about 2/3 compared with the experience reported in references 2 and 3.

A listing of the latest FORTRAN program used in the wall setting process is shown in Appendix A. This program is now run on a PDP 11-45 computer.

Two Data Input files are required:-

1) The imaginary wall velocities and the corresponding wall contours, called up for the current tunnel run as a result of previous computations.

2) The pressure data from the current run for both the flexible walls and the airfoil.

Normally the first file has been created by the previous run of the program, and therefore only the second file has to be typed in manually for each run. Program outputs are printed as follows.

1) C_p values over the airfoil, and the chord Reynolds number of the run.

2) The jack movements for both flexible walls required before the next tunnel run, and the corresponding imaginary (external) wall velocities which will exist over the next wall contours.

The computer also creates a Data Output File, into which are fed the imaginary external wall velocities and the wall contours which will be required in the analysis of the next run.

This method for analysing the SSWT wall data has proved to be fast. The latest wall setting strategy has reduced significantly the number of required iterations, and this combined with the much more rapid computations which are now being experienced on the PDP 11-45 has reduced massively the average time to streamline the walls, from about 1440 minutes to about 240 minutes. The latter figure is of course still much too high. The largest inroads into it will be made by automating the setting of the walls and acquisition of pressure data, while further progress might still be made in reducing the average number of iterations. Such advances could result in a reduction of streamlining time to the order of 2 minutes.

4. DESIGN ANALYSIS

FOR TRANSONIC SELF-STREAMLINING TEST SECTION

4.1 Jack Setting Accuracy

The analysis of the effects of wall setting errors in reference 3 gave guidance on the selection of the required setting accuracy. With the Transonic Self-Streamlining Tunnel (TSST) an accuracy of ±0.127mm. (±.005 inches) has been chosen as a target value, and some effort has been expended to check that this is achievable.

The jack design for the TSST ensures that backlash (or free-play) in the mechanical drive does not affect the accuracy of the position measurement, since the position transducer (a linear potentiometer) is almost directly coupled to the flexible-wall. The word 'almost' appears because of the presence of flexures between the transducer and wall.

The accuracy with which the wall position is known is dependent on the resolution of the linear potentiometer and on the effect of flexure distortion. The calibration of the linear potentiometer has shown that its resolution introduces a probable maximum uncertainty in wall position of about 0.038mm. (.0015 inches), which is well within the required tolerance band.

Distortion of flexures will occur when the walls are streamlined, mainly due to the streamwise movement of the walls when curved. The effect will be a maximum at the downstream end of the 112cm. (44 inch) long test section,

as the upstream ends are anchored. The estimated maximum foreshortening of a flexure due to this effect is 0.068mm. (0.0027 inch).

The sum of these errors, .106mm. (.0042 inch) is inside the tolerance. However, the option still remains to estimate the magnitude of the flexure distortion since the wall contour is always known, allowing the wall position to be estimated to a higher level of accuracy.

4.2 Comparisons Between the Contours of Structural Members and Streamlines

A flexible wall is a structural member constrained by the jacks to pass through discrete points on a streamline. The contour of the wall is determined by, among other things, its elastic properties, and will presumably depart from a streamline contour between jacks because its natural elastic contour may not be the same as the streamline contour. Its contour will be modified by stiffnesses in the jack-to-wall attachments, by static pressure differences across the wall, and by friction between the flexible wall and rigid sidewalls. In the two flexible walled test sections so far designed at Southampton University the magnitudes of differences between wall and streamline contours have been minimised by:

1) grouping the jacks closely together, with the closest spacing where the greatest curvature of the wall occurs,
2) employing flexures as jack-to-wall attachments, the stiffness of the flexures being very much lower than that of the wall,

3) arranging for the pressures inside and outside of the flexible walls to be nominally equal,
4) employing feathered-edge rubber seals between the flexible walls and sidewalls.

These design features can only minimise but not eliminate the differences between the achieved contour and the streamline. In particular the natural elastic shape will inevitably differ from the streamline.

Analysis of this problem has begun. Ideally some theoretically determined streamlines likely to be experienced in airfoil testing should be considered. However, as these were not immediately available the analytical methods were developed using streamlines from simple potential flow around a realistically sized bluff body. The method is outlined below and some results given for this simple body and flowfield, but the work continues with the method being applied to the flow around an airfoil, and will be reported later.

The deflection δ produced by a series of concentrated loads acting on a nominally straight beam with its ends simply supported is given by

$$\delta = \frac{1}{EI} \int_0^{\ell} M_1 M_2 dX \qquad 4.1$$

where E = Youngs Modulus of elasticity.

I = Second moment of area of beam cross-section.

M_1 = Bending moment at X due to the applied loads.

M_2 = Bending moment at X due to a unit load applied at the point where δ is required.

In this case the deflections of several points along a beam are known but the loads generating them are not. Therefore a set of n equations for the n deflections each in terms of the n unknown loads may be solved for the loads. The deflection of any point on the beam may then be determined.

In the analysis reported here the shape was determined of a beam passing through six equally spaced points along a streamline, (hence n = 4), and the difference between the beam at its mid-point and the streamline examined. The flowfield was that around a lifting cylinder with wake; streamline contours were computed above and below the cylinder for the beam analysis. Variables included the jack spacing and the fore-and-aft position of the mid-point of the beam relative to the cylinder.

The maximum differences between beam mid-points and the streamlines occur when the mid-point is near to the model, and with large jack spacings. On figure 4.1 is shown an example of this analysis applied to the top and bottom walls, with the beam mid-points above and below the cylinder. The difference between the beam mid-point and the streamline is presented as an error, for each wall, as a function of the ratio

$$\frac{\text{jack spacing}}{\text{test section height}}$$

Shown also is a tolerance band indicating the maximum errors which are being aimed at in the design. In this example the maximum permissible jack spacing would be about 30% of the test section height.

This example is purely illustrative of the method which is currently being applied to walls and streamlines around a lifting airfoil. A study such as this of the difference between beam and streamline contours is fundamental to the design of flexible wall test sections.

4.3 Cancellation of Interference due to Length Truncation

4.3.1 It has been argued[3,4] that the finite lengths of the streamlined walls introduce an interference at a lifting model placed centrally in the test section, the interference having the form of a camber induced by flow curvature. An estimate of magnitude of the error ΔC_{Lc} due to flow curvature is[3,4]

$$\frac{\Delta C_{Lc}}{C_L} = -\left(\frac{c}{h}\right)^2 \frac{a_1}{2\pi} f\left(\frac{a}{h}\right) \qquad 4.2$$

where C_L = lift coefficient

c = wing chord

a_1 = lift curve slope

a = test section semi-length

h = test section depth.

This expression predicts an error in C_L of order 1% for the low speed test section currently in use. The

interference is small and may be correctable, but the fact of its existence has led to the proposition of methods by which the interference might be alternatively determined or even eliminated.

4.3.2 The source of interference

Before embarking on an outline of the proposed methods it is first necessary to describe the source of the interference and also describe reasons for uncertainties in the magnitude of the correction predicted by equation 4.2 above. The analysis[1] assumes the boundaries between the real and two imaginary flowfields to comprise unloaded streamlines through the test section, with free-streamwise rigid partitions existing between the flowfields and extending from near the four ends of the unloaded streamlines outwards to infinity. The partitions are intended to represent the flow constraints imposed on the real part of the flowfield by the contraction and first diffuser. A detail of the flow around the ends of the upstream partitions is shown on Figure 4.2. The partitions are loaded by an amount necessary to eliminate in those regions the upwash that would have been introduced by the lifting model in an unbounded airflow. The vorticity distribution along one partition is indicated, its sense being opposite to that of the model. The streamlines dividing the resultant flowfields in the region of the test section spring from stagnation points on the partitions. While in this flow model the ends of the partitions are clearly defined and

can be related to the appropriate end points of the contraction and diffuser, the geometries of flexible walls cannot follow the dividing streamline nor can the real flow negotiate the direction changes on and around the partitions without separations.

A closer approximation to the manner in which the wind tunnel is currently being operated is illustrated by the detail of a fixed partition/flexible wall juncture shown on Figure 4.3. An unloaded portion of flexible wall which extends along the majority of the test section is shown blending in a flexible adapter section gradually into the contraction from which it is cantilevered. The contraction still introduces in effect two loaded partitions between real and imaginary flows. An indication of the variation of loading along the test section wall is the vorticity distribution shown in schematic form; the distributions of velocity perturbations from the freestream value either side of the partition are also shown.

In applying the interference analysis[3,4] it is clearly wrong to assume the streamwise partitions to extend to the junction between the flexible adapter and unloaded wall: an overestimate of the interference effect is inevitable. For the low speed test section, equation 4.2 would predict $\frac{\Delta C_{Lc}}{C_L} = 1.03\%$. Likewise the unloaded wall cannot be assumed to extend right to the contraction: the vorticity along the adapter section would be omitted with the probability of an underestimate of the interference. Equation 4.2 would predict $\frac{\Delta C_{Lc}}{C_L} = 0.52\%$.

The options open seem to be either:

1) to accept the interference but to keep it small by suitable proportioning of the test section and make no correction,

2) to apply a correction such as given by 4.2 with a judicious choice of assumed length of test section,

3) to devise alternative methods of accounting for truncation effects.

The next section outlines a possible line of approach for the latter option.

4.3.3 Proposed method for eliminating truncation interference effects

This small interference might be eliminated by the deliberate introduction of wall vorticity of appropriate sign to cancel the effects of what is being called here the partition vorticity. In order to most effectively perform its function the cancelling wall vorticity should be sited as closely as possible to the partition vorticity, consequently it is proposed that the possibility of inducing the vorticity in the four adapter sections be explored. On the upper half of Figure 4.4 is shown one of these adapter regions (on the upper flexible wall at its upstream end) with some proposed modifications which might allow the generation of a controlled amount of cancelling vorticity. The wall is shown with an extra jacking point and two extra wall static pressure orifices. The wall is deformed concave downwards by the new

jack to give a contour intended to induce, in comparison with what has been the practice to the present time, a region of relatively low velocity on its real side and high velocity on its imaginary side.

The distributions of velocity perturbation from free stream on each side of the contraction partition and flexible wall are indicated. The vorticity implicit in the velocity imbalance at A is that responsible for the model interference. The proposal is that the deformation of the adapter sections should induce levels of vorticity of opposite sign at B just sufficient to eliminate induced camber at the model.

The complete test section with portions of partitions representing the contraction and diffuser is shown schematically on Figure 4.5. The senses of the vorticity are indicated on the partitions and adapter sections in the presence of model wing vorticity.

It is proposed to pursue this technique in the near future both analytically, and experimentally using the low speed self-streamlining wind tunnel. At the present time no difficulty is seen in determining the imaginary side perturbation velocities, but the feasibility of generating and then measuring or otherwise determining the real side perturbations has not yet been investigated.

5. TRANSONIC SELF STREAMLINING TEST SECTION

5.1 Wall Jack Prototype Rig

The nature of a flexible wall test section with its many jacks dictates the duplication of many components. In the case of the Transonic Self Streamlining Tunnel (TSST) there will be forty jacks, and the introduction of electro-mechanical jack control into the design. It was decided to build a prototype rig of a single jack, to test the envisaged mechanical and electrical systems.

The resulting hardware is shown photographically in Figure 5.1, the views being dominated by the simulated wind tunnel sidewalls and their supporting channel. The direction of the wind tunnel air flow can be regarded into the photograph while the base board is the centreline of the tunnel. It can be seen that the jack is connected to a length of flexible wall, the wall being made of Polyester Reinforced Acrylic Laminate, which in this rig is restrained one model chord length (7.6cm., 3 inches) either side of the jack. Also fitted are the rubber seals between the tunnel side walls and the flexible wall. The jack is connected to the rib on the flexible wall by means of two rods with thin flexures. The rods pass through 'O' ring seals in the supporting channel, to a connecting bar. Seals are needed because the volume between the flexible wall and the supporting channel will in operation be below atmospheric pressure so as to relieve the pressure forces on the flexible wall.

The jack lead screw and position transducer are applied to the connecting bar. The former is driven by a stepper motor via a worm reduction gear and flexible coupling. The linear position transducer is simply held in contact with the connecting bar by a spring, to measure jack movement relative to a datum position.

The principal aim of the prototype rig was to demonstrate jack performance under realistic conditions, hence the inclusion of all the seals and dummy adjacent jacks. A maximum jack force requirement of order 110N (25 lb) had been calculated, with reserves. Existing theoretical and experimental data indicated that the maximum required jack movement would not exceed one inch. These figures were used as a basis for the mechanical design of the rig.

The drive system centers on a stepper motor because these can be easily controlled in closed loop operations. The actual motor chosen is a 3-phase Slo-Syn, type M051-DW601, which provides 24 steps per revolution, i.e. 15^{o} per step. This is coupled to a 25:1 worm wheel reduction gearing and a lead screw of 26 threads per inch, to achieve sufficient force and fine movement control at the jack.

A Sakae 20 LP 30 linear displacement potentiometer has been chosen. This type was expected to meet the target accuracy of ±.127mm. (±.005 inch) and also be capable of accommodating the envisaged jack movements, having a measurement travel of 30mm. (1.18 inches). A three-phase motor drive logic system was developed for this rig, allowing

selection of motor movement in either direction and at a wide variety of stepping rates up to the maximum tolerated by the motor. Each view on Figure 5.1 shows the jack driven to a position of maximum deflection as limited by lead screw length, potentiometer travel and wall deflection.

Of importance is the time taken for the flexible walls to adjust. It was found that the jack could be moved at rates up to approximately 0.43mm. (0.017 inch) per second. On a flexible walled test section a wall movement of 5mm. per iteration is large, therefore wall re-positioning will require less than 12 seconds motoring time per iteration.

The linearity of the position transducer was investigated with the rig, and the resulting calibration over the complete travel is shown in Figure 5.2. The maximum recorded error was 0.038mm. (.0015 inch) and in fact the overall linearity and hysteresis where better than stated in the manufacturer's specifications.

Throughout the tests there were no problems with the flexible wall, and it proved very strong and plyable; the stepper motor would stall with no sign of the wall breaking. It was also shown that the motor could impose the necessary strong curvature on the wall, and that the flexures could withstand full compressive jack force.

As a result of the confidence gained with the mechanical design of the jack and the three phase control logic for the stepper motor, the designs have formed the subsequent pattern of the complete transonic test section.

5.2 Transonic Test Section Design

Views of this design are given on Figure 5.3, from which the main design features will be self evident. The test section is 15¼cm. (6 inches) wide and is shown at a nominal depth of 7.6cm. (3 inches). Provision is made for varying the depth from this value to a maximum of 15.2cm. (6 inches). There are 20 jacks per wall, each with its own drive motor, position transducer and wall static pressure orifice. The flexible wall material is laminated fiber and is relatively lightly loaded, being vented on its jack side to the test section downstream of the model. The two-dimensional wing models will be mounted from trunnions in the sidewalls. There are Schlieren-quality glass windows in the sidewalls at the model location. The sidewalls have no boundary layer treatment.

The test section forms an insert to an existing induced-flow tunnel working at normal temperature and at a stagnation pressure of one atmosphere. Flow Mach numbers in excess of unity are possible with an empty test section, although with a model present a lower limit will be set by the interception of wing shocks with the walls.

The test section is in manufacture at the present time, and the tunnel area is being prepared. The anticipated date of completion of the mechanical construction is May 1977.

6. CONCLUSIONS

1. Good agreement with unstalled interference-free data has been obtained on a NACA-0012 airfoil in the self streamlining test section, but agreement is poor in the stall region.

2. A new method of rapid wall adjustment has been developed resulting in the need for only one iteration step in some tests.

3. The wall setting strategy and new computer program has allowed a significant reduction in the time required for streamlining, from about 1440 minutes to about 240 minutes.

4. The causes of flexible wall position errors have been investigated, and the errors are shown to be acceptably small.

5. It may prove possible to reduce the small interference effect of test section truncation.

6. The transonic self streamlining test section now under construction is designed to reduce streamlining times to less than 2 minutes.

```
********** LISTING OF XSW1.FTN **********

      DIMENSION AA(300),BB(300),CC(300),CB(128),ICB(32)
      DIMENSION B(40),D(20),X(20),W(20),Y(20),G(20),P(25),U(20),Q(20)
      DIMENSION V(20),E(20),H(20),C(18,4),Z(18),S(18),T(18),RS(18)
      DIMENSION N(18),A(4),XB(4)
      EQUIVALENCE (CB(33),ICB(1))
      REAL N
      CALL TYPE('&          WALL ANALYSIS')
      CALL TYPE('&           **********')
      CALL ASKN(AA,'&          WALL DATA INPUT FILE =')
      CALL ASKN(BB,'&        PRESSURE DATA INPUT FILE =')
      CALL ASKN(CC,'&           DATA OUTPUT FILE =')
      CALL INPUT (AA,CB,MA)
      ASSIGN 1000 TO MA
      CALL INPUT (BB,CB,MB)
      ASSIGN 1001 TO MB
      CALL OUTPUT (CC)
      CALL INS(AA,0,0)
      CALL INS(BB,0,0)
      DO 10 J = 1,18
   10 CALL IN(AA,RS(J))
      DO 20 J = 1,18
   20 CALL IN(AA,N(J))
      DO 30 J = 1,20
   30 CALL IN(AA,X(J))
      DO 40 J = 1,20
   40 CALL IN(AA,W(J))
      DO 50 J = 1,25
   50 CALL IN(BB,P(J))
      DO 60 J = 1,20
   60 CALL IN(BB,Q(J))
      DO 70 J = 1,40
   70 CALL IN(BB,B(J))
      DO 80 J = 1,20
   80 CALL IN(BB,D(J))
      CALL IN(BB,AK1)
      CALL IN(BB,AK3)
      AK2 = AK1
      AK4 = AK3
      M = 20
      AK = 0.053741
      P(22) = P(21)*AK
      CALL TYPE('&&&      AEROFOIL PRES. DIST. FOR RUN')
      K = P(25)
      CALL TYPEI(K)
      CALL TYPE('&      ********************************')
      CALL TYPE('&        ORIFICE           PRES.COEF.')
      DO 90 J = 1,39
      P1 = (B(40)-B(J))/(0.949*B(40))
      CALL TYPE('&           ')
      CALL TYPEI(J)
      CALL TYPE('           ')
   90 CALL TYPER(P1)

******** 'RETURN' ONLY = CONTINUE ,'CHAR''RETURN' =EXIT ********
```

********** LISTING OF XSW1.FTN **********

```
      CALL TYPE('&&&              INPUT CONDITIONS')
      CALL TYPE('&       X(IN)     UPPER VEL.   LOWER VEL.')
      CON1 = (1+AK)/P(1)
      CON2 = (1+AK)/Q(1)
      DO 100 I = 1,M
      CALL TYPE('&')
      CALL TYPER(D(I),X(I),W(I))
      TEMP = SQRT(CON1*P(I)-AK)-1
      U(I) = TEMP-X(I)
      E(I) = (AK3*U(I)/2)+X(I)
      TEP = SQRT(CON2*Q(I)-AK)-1
      V(I) = W(I)-TEP
  100 H(I) = W(I)-(AK4*V(I)/2)
      L = M-2
      DO 110 I = 1,L
  110 Z(I) = (D(I)+D(I+1))/2
      CALL TYPE('&   CHORD REYNOLDS NO. =')
      D1 = P(23)*0.022855/(273.15+P(24))
      U0 = SQRT(8.333*(P(21)-P(22))/D1)
      R2 = U0 * D1*32180*1000/(11.52+0.034*P(24))
      R3 = R2*5.4/12
      CALL TYPER(R3)
      NC = 0
   65 I = 0
   35 DO 120 J = 1,4
      KI = I+J
      IF (KI.LT.3) GO TO 5
      IF (KI.GT.3) GO TO 5
      A(J)= (D(I+J)-0.3)
      GO TO 15
    5 A(J) = (D(I+J)+0.2)
   15 IF (NC.EQ.0) GO TO 25
      XB(J) = V(I+J)
      GO TO 120
   25 XB(J) = U(I+J)
  120 CONTINUE
      V0 = (XB(3)-XB(2))/(A(3)-A(2))
      V1 = XB(2)-V0*A(2)
      V2 = 1/(A(4)-A(1))
      V3 = (XB(4)-V0*A(4)-V1)/((A(4)-A(2))*(A(3)-A(4)))
      V4 = (XB(1)-V0*A(1)-V1)/((A(1)-A(2))*(A(3)-A(1)))
      V6 = V2*(V3-V4)
      V5 = V4-V6*A(1)
      I = I+1
      C(I,1) = V1-A(2)*A(3)*V5
      C(I,2) = V0+V5*(A(2)+A(3))-V6*A(2)*A(3)
      C(I,3) = V6*(A(2)+A(3))-V5
      C(I,4) = -V6
      IF (I.LT.(M-3)) GO TO 35
      LI = M-2
      DO 130 J = 2,LI
      Z0 = Z(J)
```

******** 'RETURN' ONLY = CONTINUE ,'CHAR''RETURN' =EXIT ********

```
      SS = 0
      K = M- 3
      DO 140 I = 1,K
      Y1 =D(I+1)
      C0 = C(I,1)
      C1 = C(I,2)
      C2 = C(I,3)
      C3 = C(I,4)
      Y2 = D(I+2)
      S0 = C0+C1*Z0+C2*(Z0*Z0)+C3*(Z0*Z0*Z0)
      TEMP = ABS(Y2-Z0)/ABS(Y1-Z0)
      S1 = ALOG(TEMP)
      S2 = (C1+C2*Z0+C3*(Z0*Z0))*(Y2-Y1)
      S3 = (C2+C3*Z0)*((Y2*Y2)-(Y1*Y1))/2
      S4 = C3*((Y2*Y2*Y2)-(Y1*Y1*Y1))/3
      SS = SS+S0*S1+S2+S3+S4
  140 CONTINUE
      IF (NC.EQ.1) GO TO 45
      S(J) = SS/6.28319
  130 CONTINUE
      IF (NC.EQ.1) GO TO 75
      NC = 1
      GO TO 65
   45 T(J) = SS/6.28319
      GO TO 130
   75 R = 0
      TT = 0
      CALL TYPE('&&&          OUTPUT RUN')
      K = P(25)
      CALL TYPEI(K)
      CALL TYPE('&           ***********')
      CALL TYPE('&  JACK    X(IN)       UPPER VEL    LOWER VEL')
      CALL TYPE('      UP Y          LO Y')
      L = M-4
      DO 150 I =1,L
      T0 = S(I)
      R0 = T(I)
      T1 = Z(I)
      I = I+1
      T2 = D(I)
      T3 = S(I)
      R3 = T(I)
      T4 = Z(I)
      I = I+1
      T5 = D(I)
      T6 = S(I)
      R6 = T(I)
      T7 = Z(I)
      T8 = ((T6-T3)/(T7-T4)-(T0-T3)/(T1-T4))/(T7-T1)
      T9 = (T6-T3)/(T7-T4)-T8*T7
      P2 = (T3-T9*T4)*(T5-T2)+T8*((T5*T5*T5)-(T2*T2*T2))/3
      TT = TT+P2+(T9-T8*T4)*((T5*T5)-(T2*T2))/2

******** 'RETURN' ONLY = CONTINUE ,'CHAR''RETURN' =EXIT ********
```

```
          ********** LISTING OF XSW1.FTN **********

          R8 = ((R6-R3)/(T7-T4)-(R0-R3)/(T1-T4))/(T7-T1)
          R9 = (R6-R3)/(T7-T4)-R8*T7
          P3 = (R3-R9*T4)*(T5-T2)+R8*((T5*T5*T5)-(T2*T2*T2))/3
          F = E(I)
          R = R+P3+(R9-R8*T4)*((T5*T5)-(T2*T2))/2
          Y(I) = (AK3*TT)+(AK2*AK4*R)
          G(I) = (AK4*R)+(AK1*AK3*TT)
          E(I) = E(I) + ((H(I)-W(I)+V(I))*AK2)
          H(I) = H(I) +((F-U(I)-X(I))*AK1)
          K = I-2
          CALL TYPE('&  ')
          CALL TYPEI(K)
          CALL TYPER (D(I),E(I),H(I),Y(I),G(I))
      150 I = K
          TT = TT+S(18)*(D(19)-D(18))
          R = R+T(18)*(D(19)-D(18))
          Y(19) = TT + (AK2*R)
          G(19) = R + (AK1*TT)
          Y(20) = Y(19)
          G(20) = G(19)
          CALL TYPE('& EXIT')
          CALL TYPER(D(19),E(19),H(19),Y(19),G(19))
          CALL TYPE('&      ')
          CALL TYPER(D(20),E(20),H(20),Y(20),G(20))
          EE = 0
          F = 0
          DO 160 I = 1,M
          EE = EE+(U(I)*U(I))
          F = F+(V(I)*V(I))
      160 CONTINUE
          EE = (SQRT(EE/(M-2)))*2
          F = (SQRT(F/(M-2)))*2
          CALL TYPE ('&&          UPPER ERROR =')
          CALL TYPER (EE)
          CALL TYPE('       LOWER ERROR =')
          CALL TYPER(F)
          CALL TYPE('&           **********************')
          CALL TYPE('       **********************')
          K = P(25)+1
          CALL TYPE('&&   RUN')
          CALL TYPEI(K)
          CALL TYPE('   WALL SETTINGS')
          CALL TYPE('& JACK    DELTA        OLD        SET')
          CALL TYPE('        SET + 0.5')
          L = M-2
          DO 170 J = 1,L
          S1 = RS(J) + Y(J+2)
          CALL OUT (CC,S1)
          S2 = S1 + 0.5
          CALL TYPE ('& ')
          CALL TYPEI(J)
      170 CALL TYPER(Y(J+2),RS(J),S1,S2)

******** 'RETURN' ONLY = CONTINUE ,'CHAR''RETURN' =EXIT ********
```

********** LISTING OF XSW1.FTN **********

```
      DO 180 J = 1,L
      S1 = N(J) - G(J+2)
      CALL OUT (CC,S1)
      CALL TYPE('& ')
      CALL TYPEI(J)
180   CALL TYPER(G(J+2),N(J),S1)
      DO 190 J = 1,20
190   CALL OUT(CC,E(J))
      DO 200 J = 1,20
200   CALL OUT(CC,H(J))
      CALL INEND(AA)
      CALL INEND(BB)
      CALL OUTEND(CC,CB)
      GO TO 55
1000  CALL TYPE('&  WALL DATA ERROR DETECTED')
1001  CALL TYPE('&      PRESSURE DATA ERROR DETECTED')
55    END
```

******** END OF LISTING - PRESS 'RETURN' TO EXIT ********

SYMBOLS

a	test section semi-length
a_1	lift curve slope
a_1, a_2, a_3, a_4	scaling factors used in setting walls
c	wing chord
C_c	chordwise force coefficient
C_L	lift coefficient
C_N	normal force coefficient
C_p	pressure coefficient
E	Young's modulus
h	test section height
I	second moment of area of the beam section
ℓ	length of the beam
M_1	bending moment
M_2	bending moment due to a unit load at the point where δ is measured
R_c	Reynolds number based on wing chord
x	chordwise position downstream from the leading edge
X	lengthwise position on beam
Y_T Y_B	required local movements for top and bottom walls respectively, calculated using methods of reference 1
Y_T Y_B	local top and bottom wall movements respectively, using factors a_1 and a_2
Y_T' Y_B'	local top and bottom wall movements respectively, using factors a_1, a_2, a_3 and a_4
α	angle of attack
δ	beam deflection at a point
ΔC_{Lc}	error in C_L due to induced camber

REFERENCES

1. M. Judd, S.W.D. Wolf and M.J. Goodyer — 'Analytical Work in Support of the Design and Operation of Two Dimensional Self Streamlining Test Sections' NASA CR-145019

2. M.J. Goodyer — 'The Self Streamlining Wind Tunnel' NASA TMX-72699 August 1975

3. M.J. Goodyer — 'A Low Speed Self Streamlining Wind Tunnel' AGARD Conference Proceedings No. 174-Wind Tunnel Design and Testing Techniques, London, October 1975

4. M. Judd, M.J. Goodyer and S.W.D. Wolf — 'Application of the Computer for on-site Definition and Control of Wind Tunnel Shape for Minimum Boundary Interference' AGARD Conference Proceedings. No. 210-Numerical Methods and Wind Tunnel Testing, June 1976

Test No	α	Starting Contours	Number of Iterations
1	-6°	Straight Walls	4
2	-4°	$\alpha = -6^{\circ}$	1
3	-4°	Straight Walls	4
4	0°	Straight Walls	3
5	$+2^{\circ}$	$\alpha = 0^{\circ}$	1
6	$+4^{\circ}$	$\alpha = +2^{\circ}$	1
7	$+6^{\circ}$	$\alpha = +4^{\circ}$	2
8	$+7^{\circ}$	$\alpha = +8^{\circ}$	2
9	$+8^{\circ}$	$\alpha = +9^{\circ}$	2
10	$+9^{\circ}$	$\alpha = +10^{\circ}$	1
11	$+10^{\circ}$	Straight Walls	3
12	$+12^{\circ}$	$\alpha = +10^{\circ}$	3
13	$+12^{\circ}$	$\alpha = +12^{\circ}$	1
14	$+12^{\circ}$	Straight Walls	3
15	$+12^{\circ}$	$\alpha = +12^{\circ}$	1

Test 13 was with L.E. fences fitted.
Test 14 was with L.E. fences fitted and exit movement.
Test 15 was with T.E. fences fitted.

FIG. 2.1 SUMMARY OF SSWT TESTS.

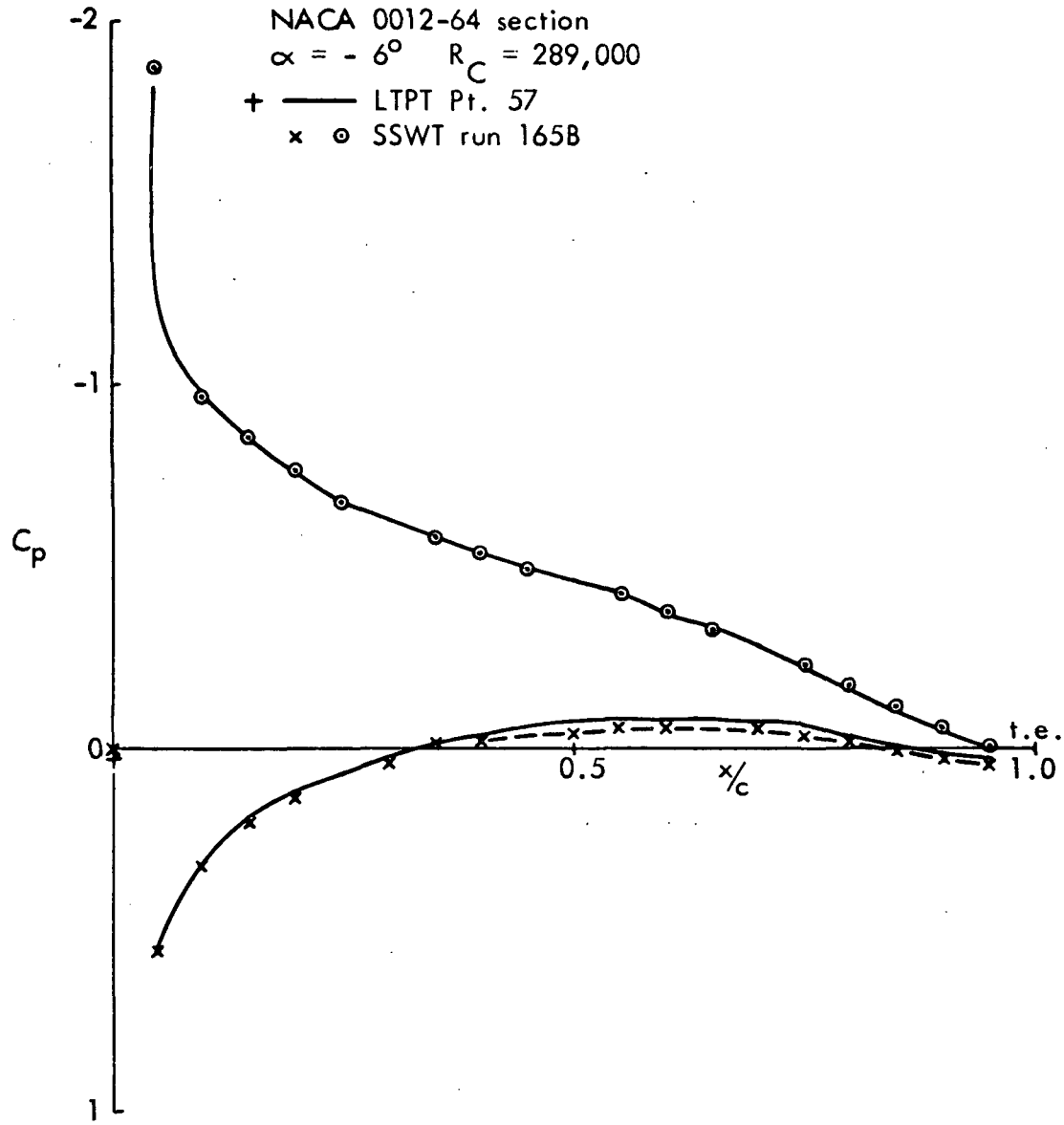

FIG. 2.2(a) TEST 1 AIRFOIL PRESSURE DISTRIBUTION

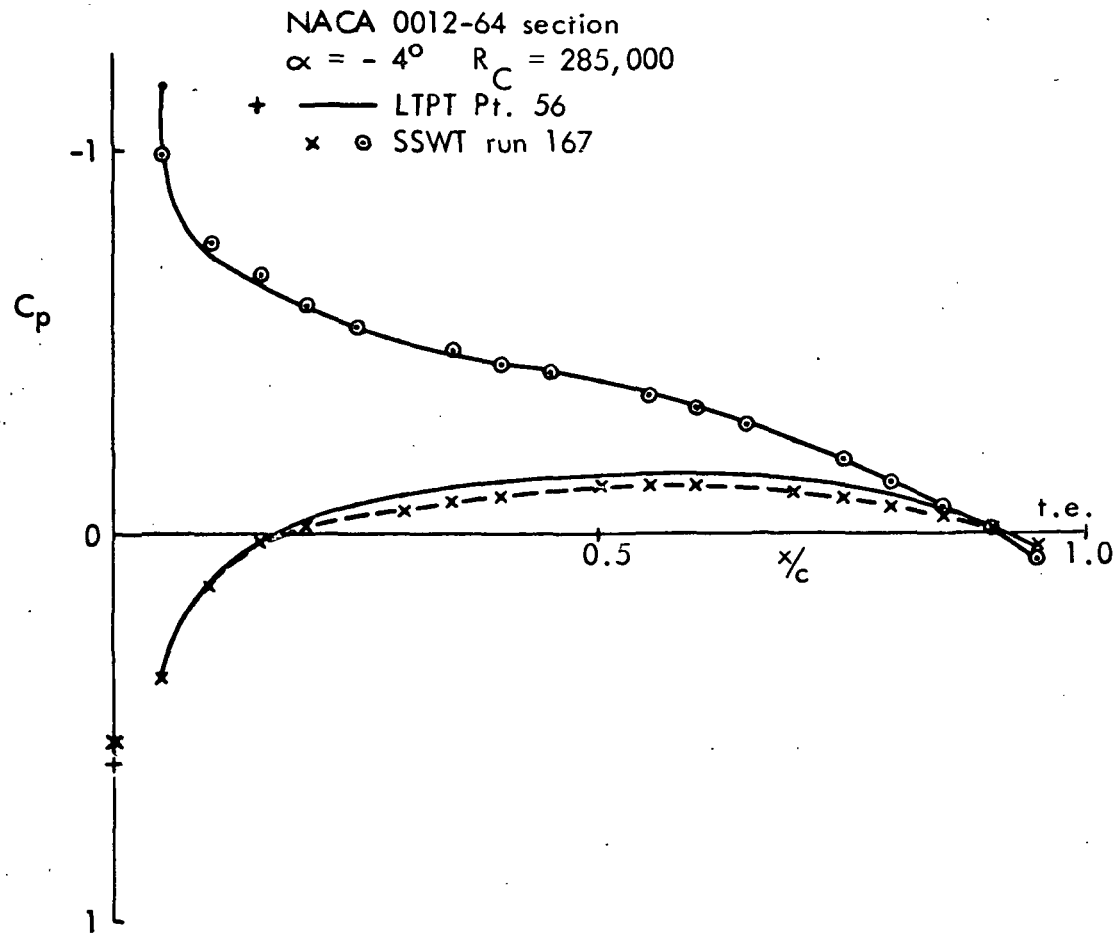

FIG. 2.2(b) TEST 2 AIRFOIL PRESSURE DISTRIBUTION

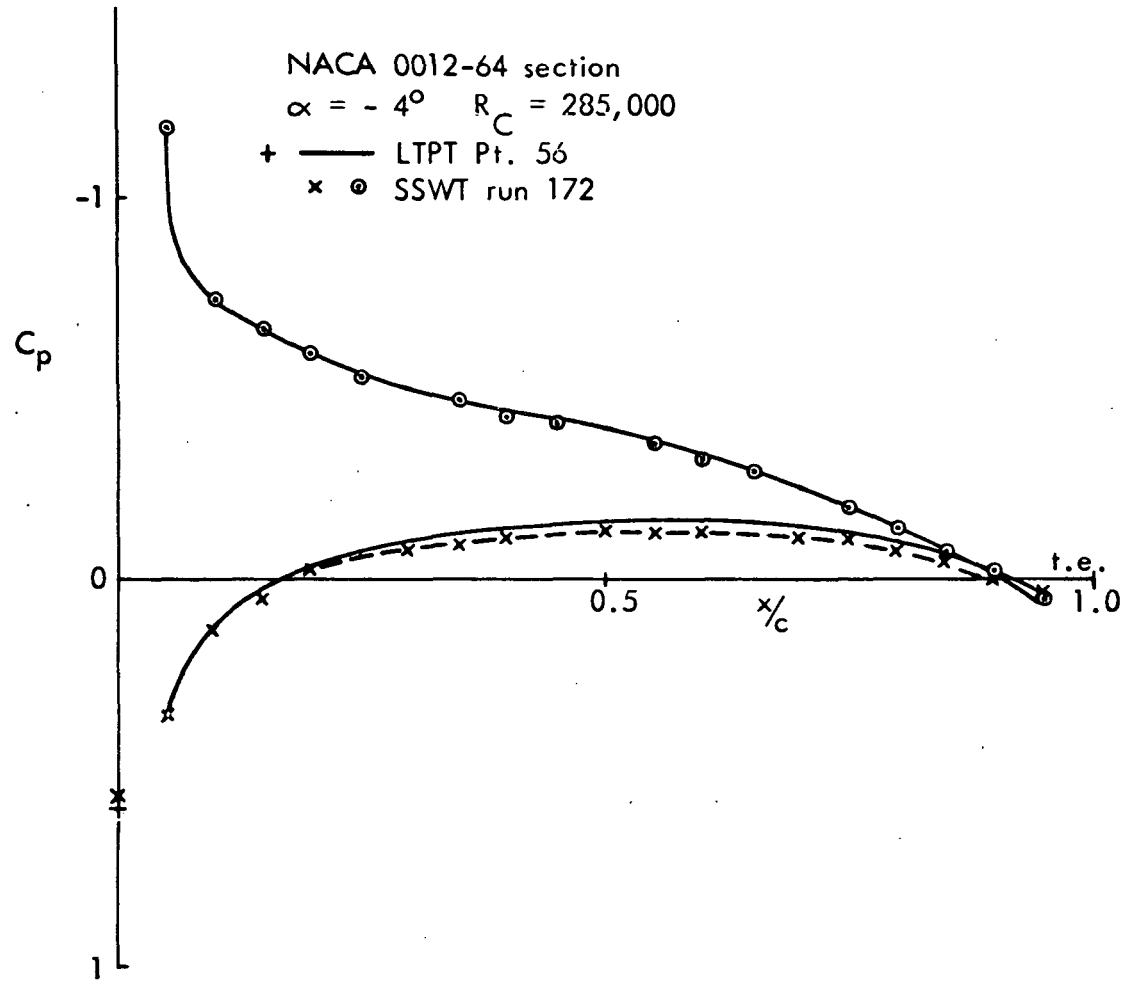

FIG. 2.2(c) TEST 3 AIRFOIL PRESSURE DISTRIBUTION

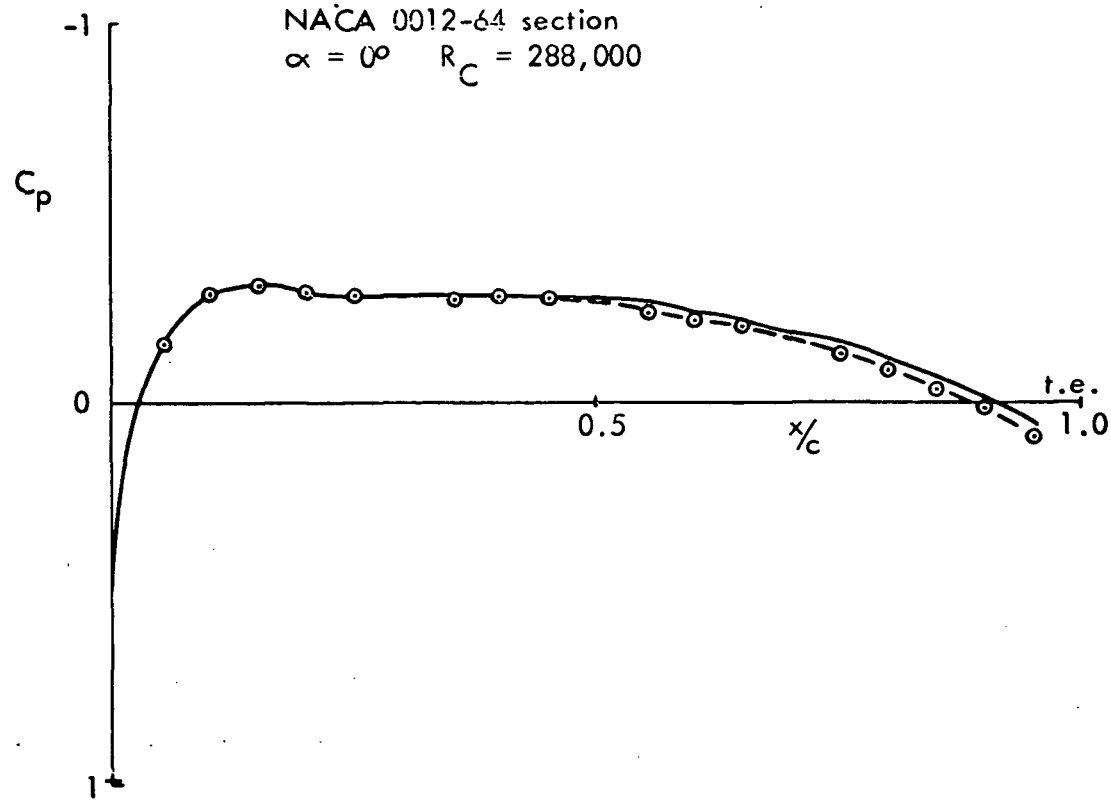

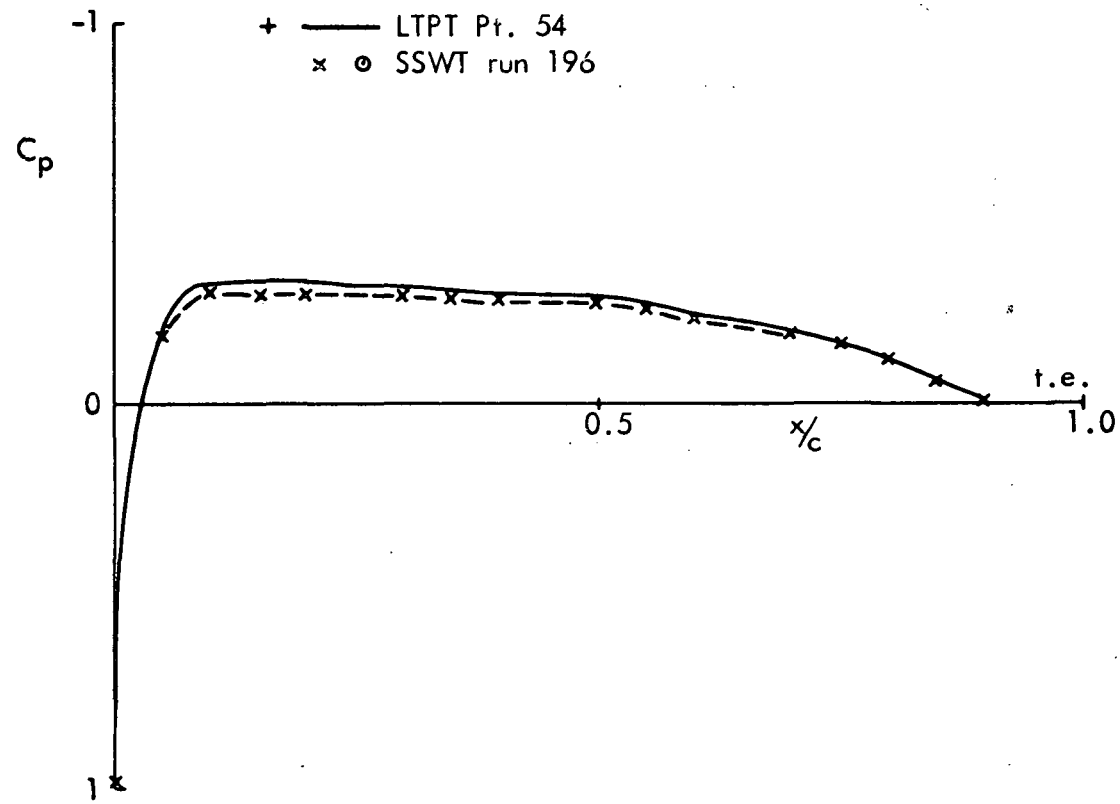

FIG. 2.2(d) TEST 4 AIRFOIL PRESSURE DISTRIBUTION

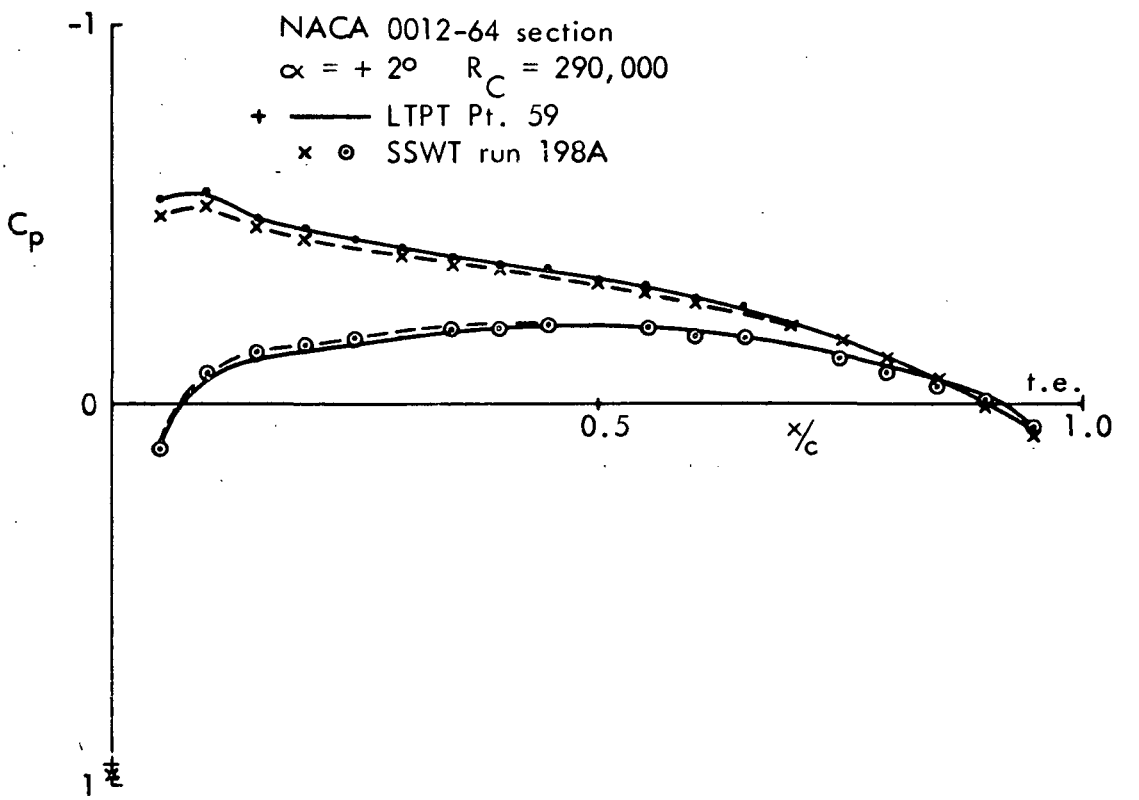

FIG. 2.2(e) TEST 5 AIRFOIL PRESSURE DISTRIBUTION

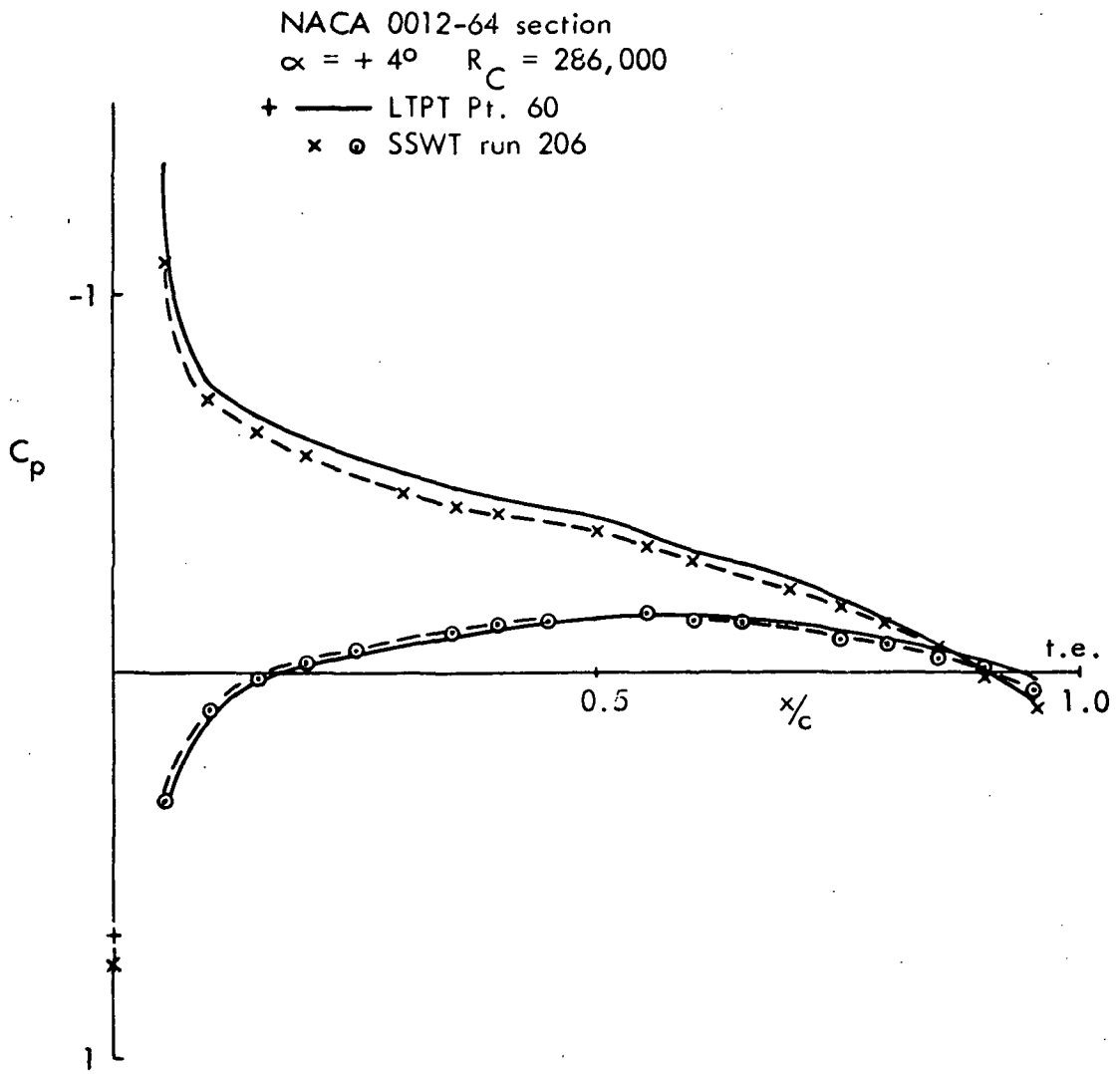

FIG. 2.2(f) TEST 6 AIRFOIL PRESSURE DISTRIBUTION

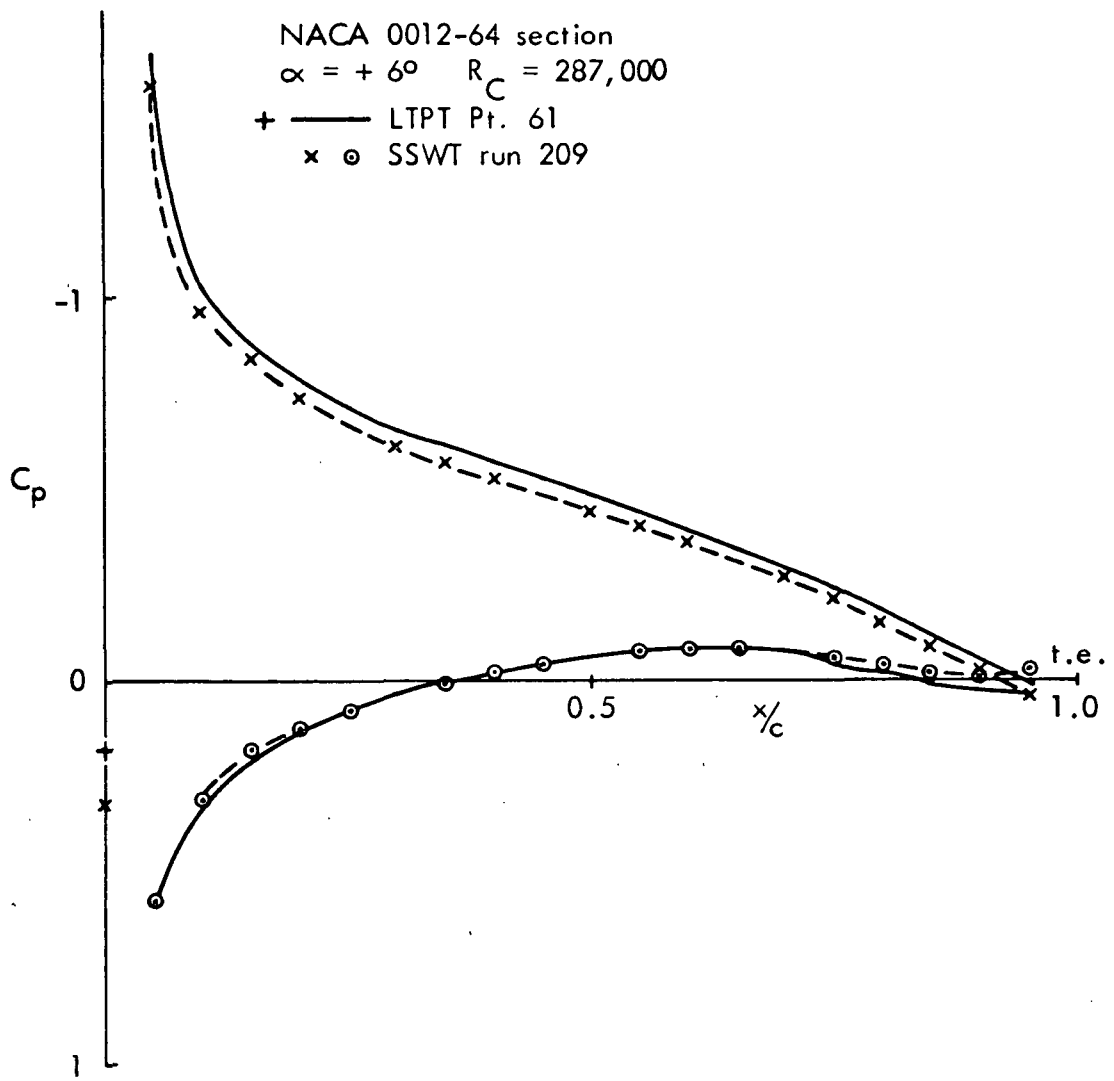

FIG. 2.2(g) TEST 7 AIRFOIL PRESSURE DISTRIBUTION

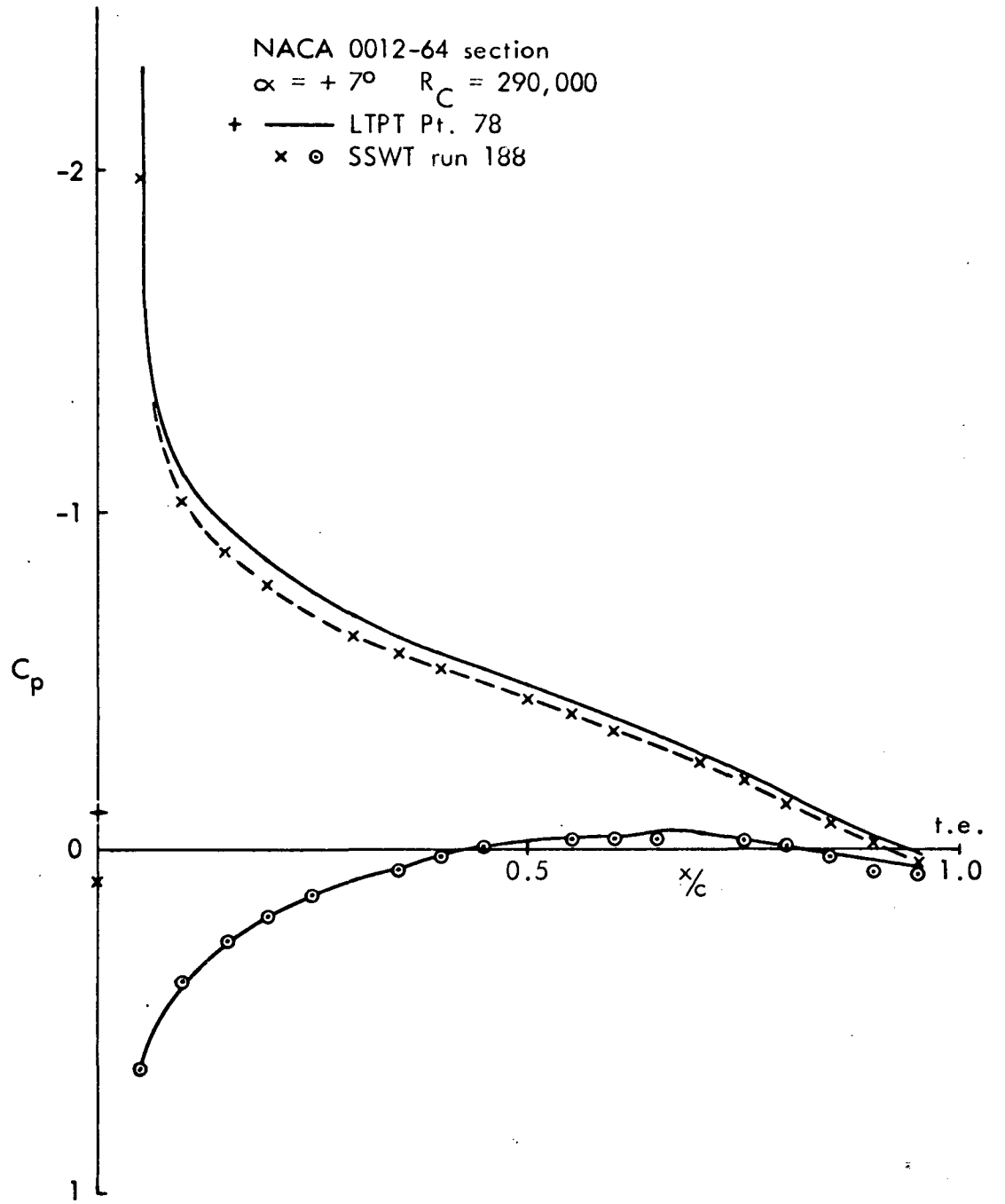

FIG. 2.2(h) TEST 8 AIRFOIL PRESSURE DISTRIBUTION

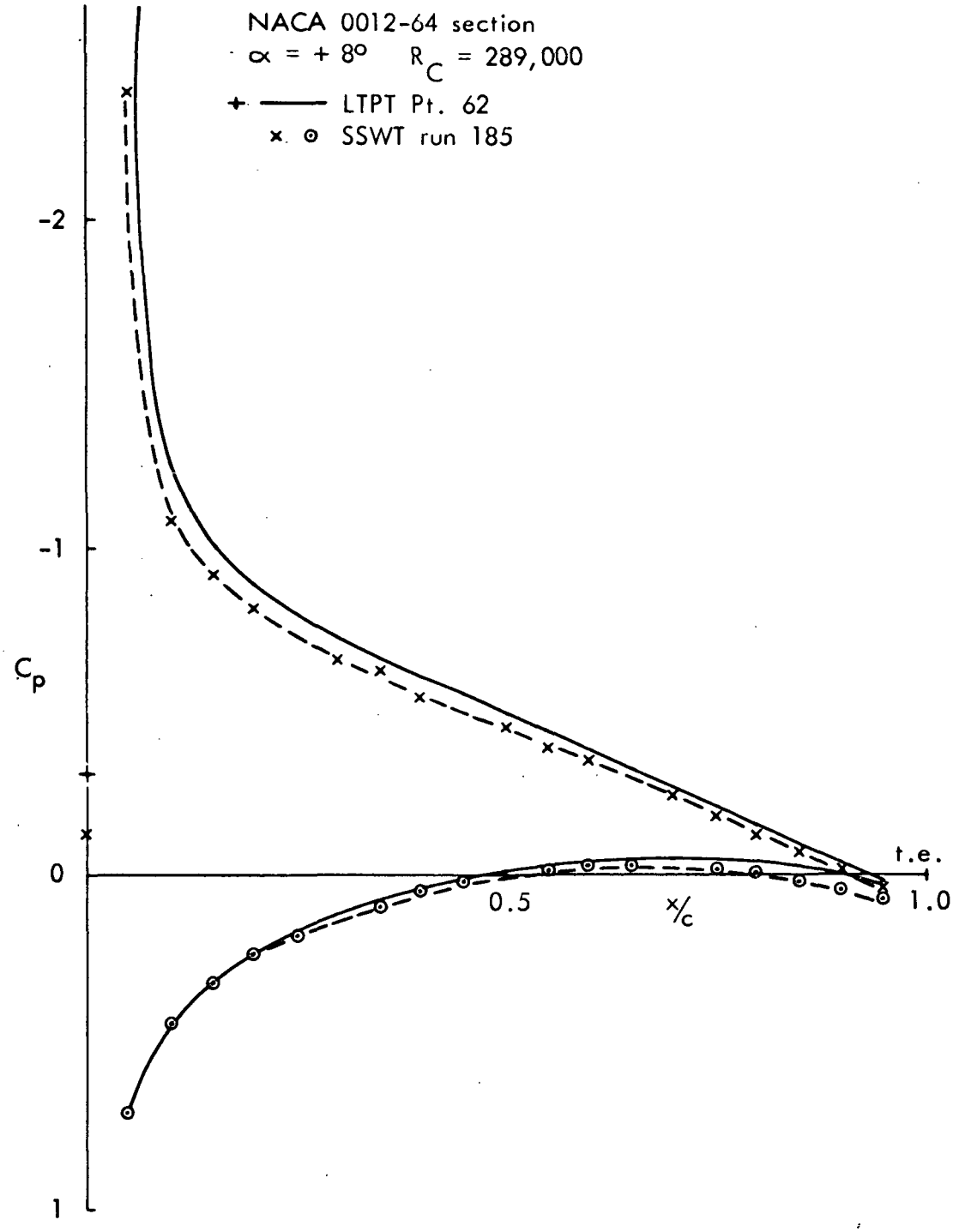

FIG. 2.2 (i) TEST 9 AIRFOIL PRESSURE DISTRIBUTION

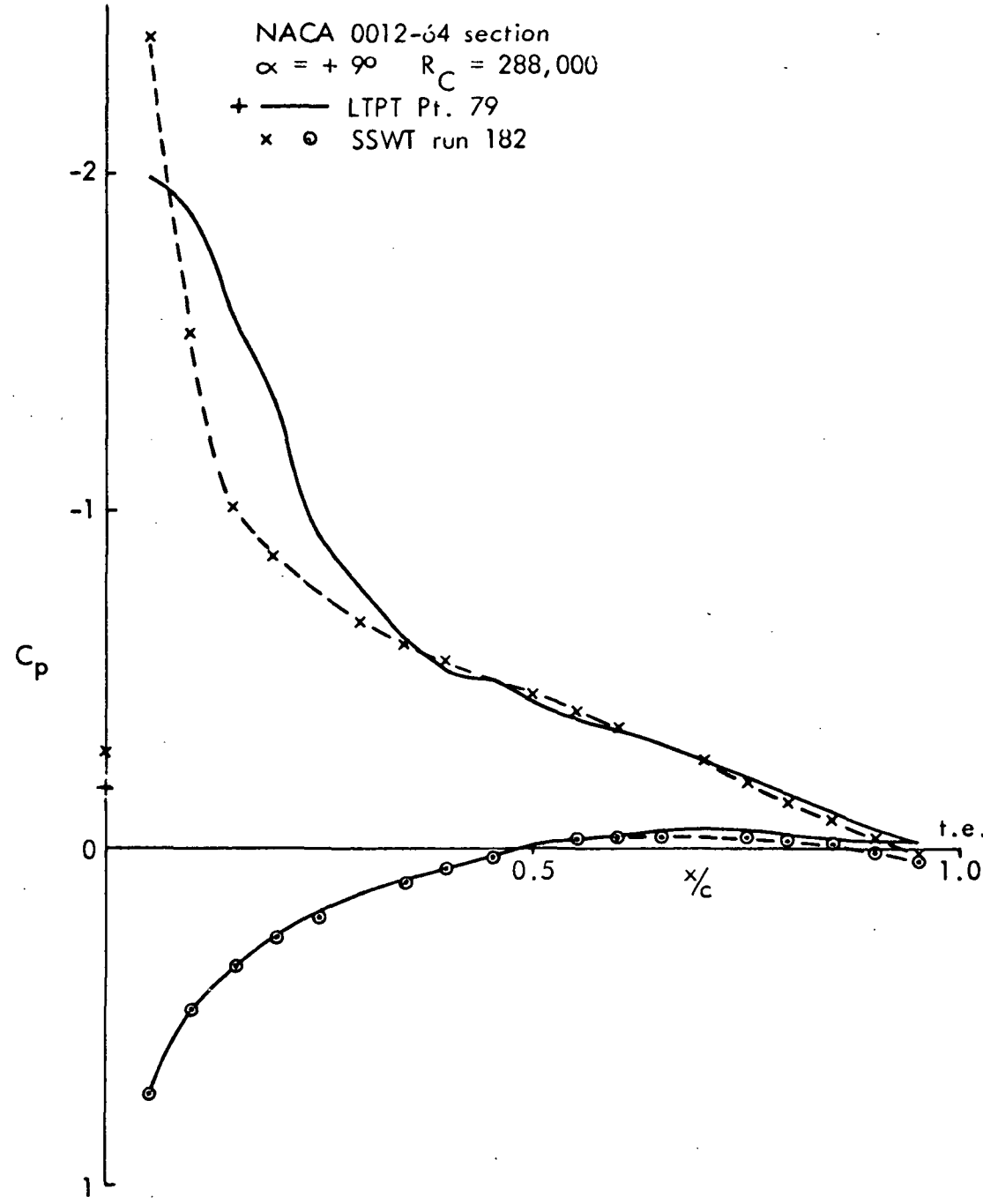

FIG. 2.2(j) TEST 10 AIRFOIL PRESSURE DISTRIBUTION

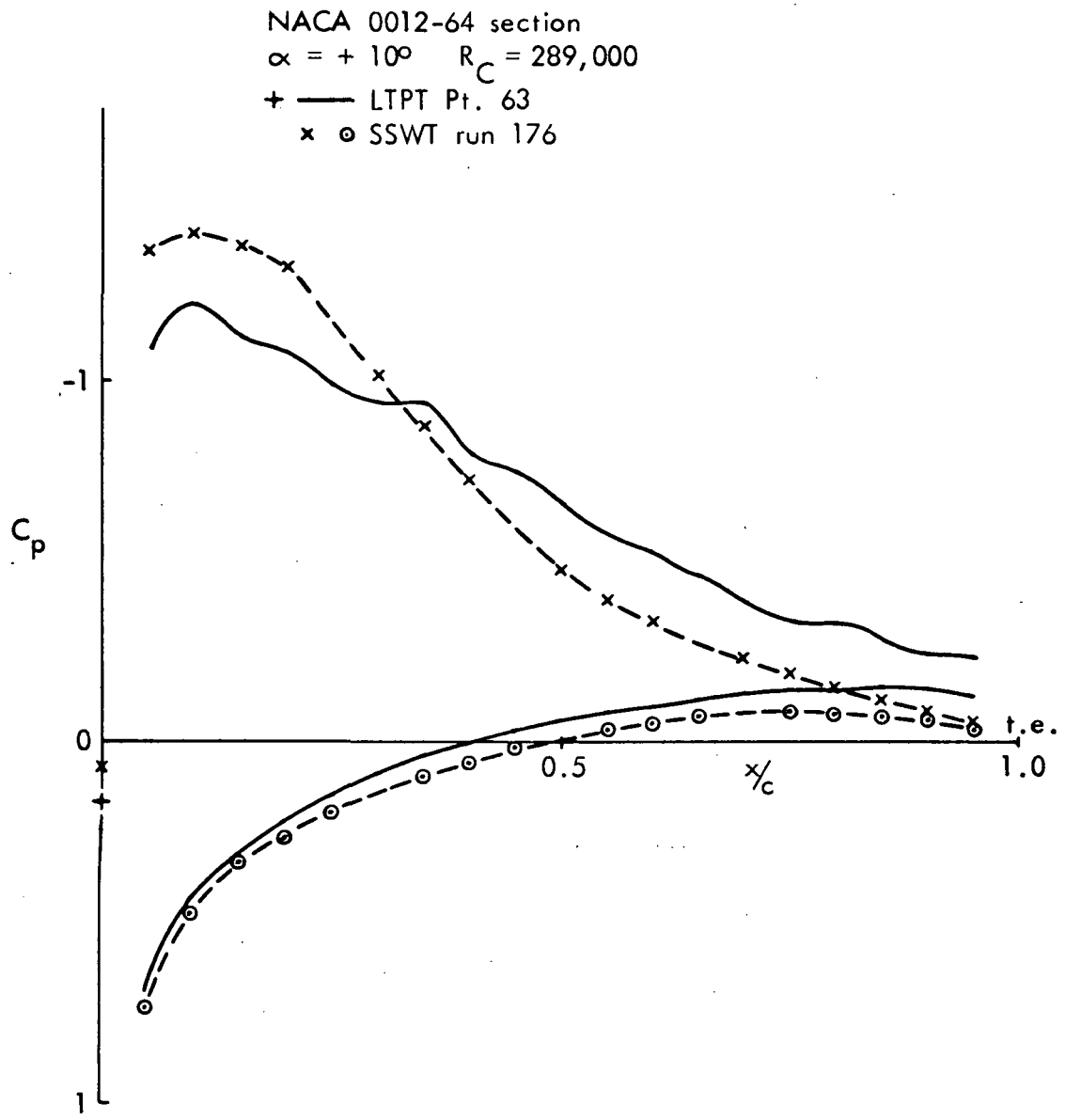

FIG.2.2(k) TEST 11 AIRFOIL PRESSURE DISTRIBUTION

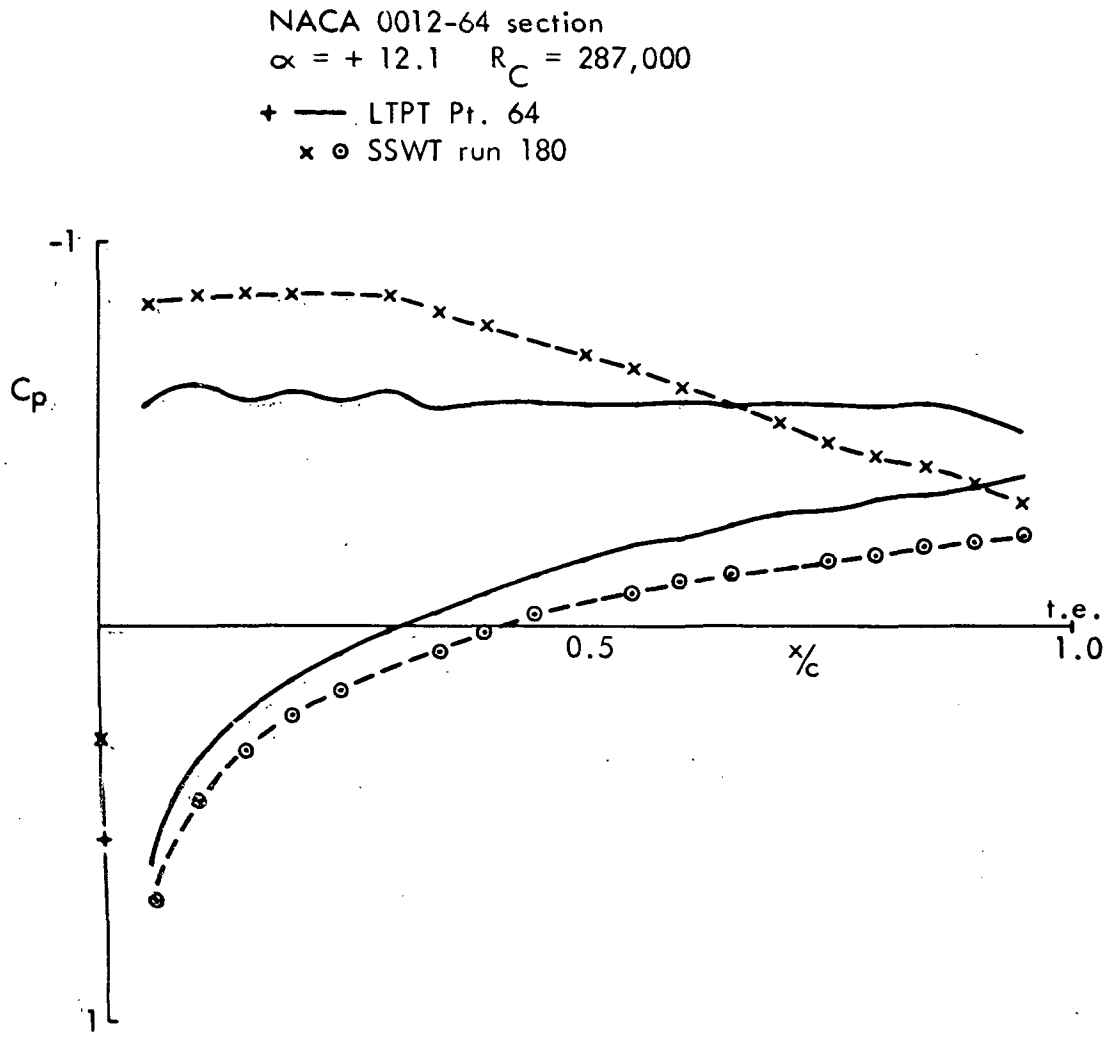

FIG. 2.2(l) TEST 12 AIRFOIL PRESSURE DISTRIBUTION

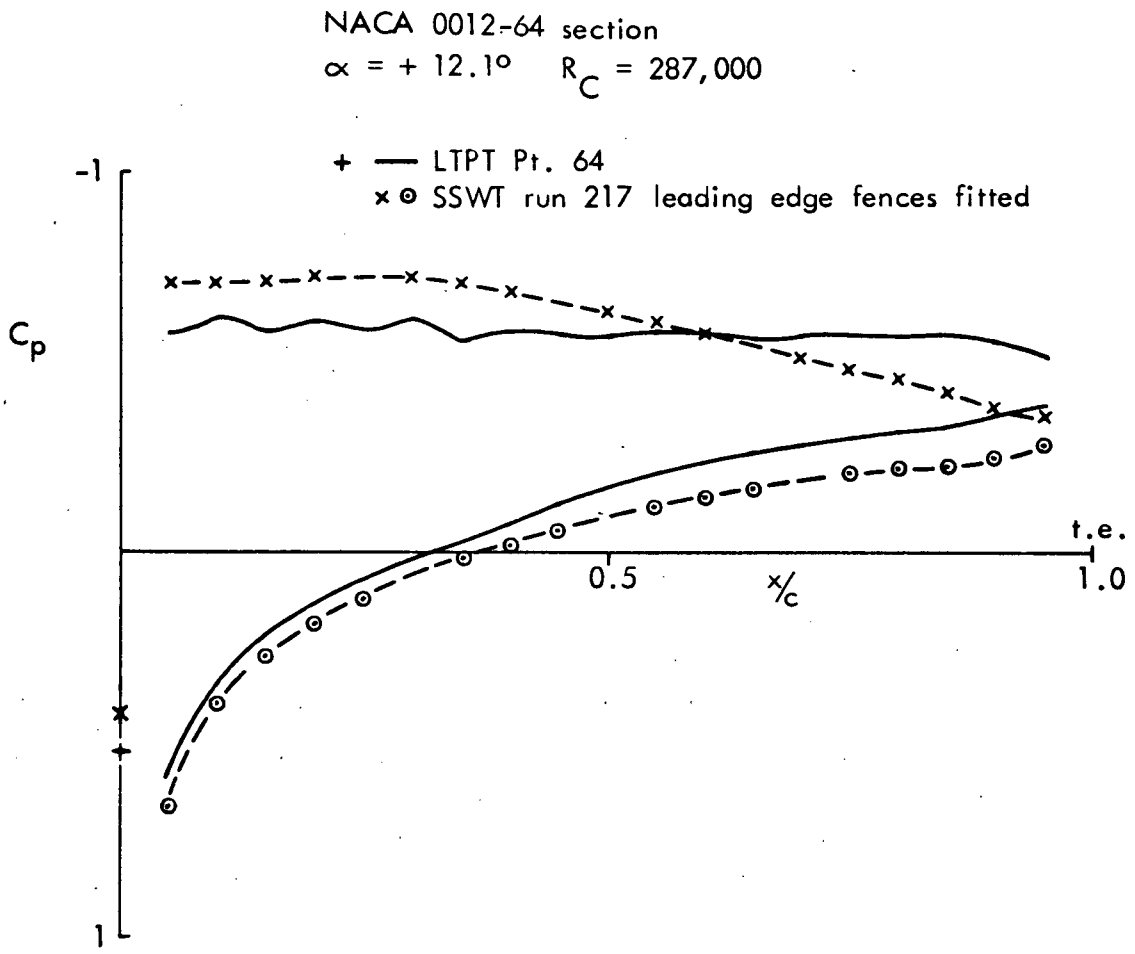

FIG. 2.2(m) TEST 13 AIRFOIL PRESSURE DISTRIBUTION

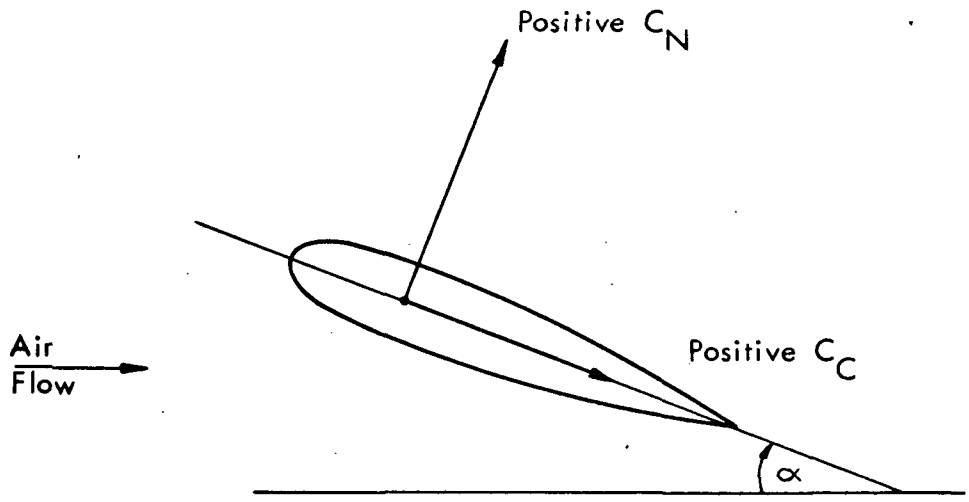

FIG. 2.3 FRAME OF REFERENCE FOR C_N AND C_C DATA

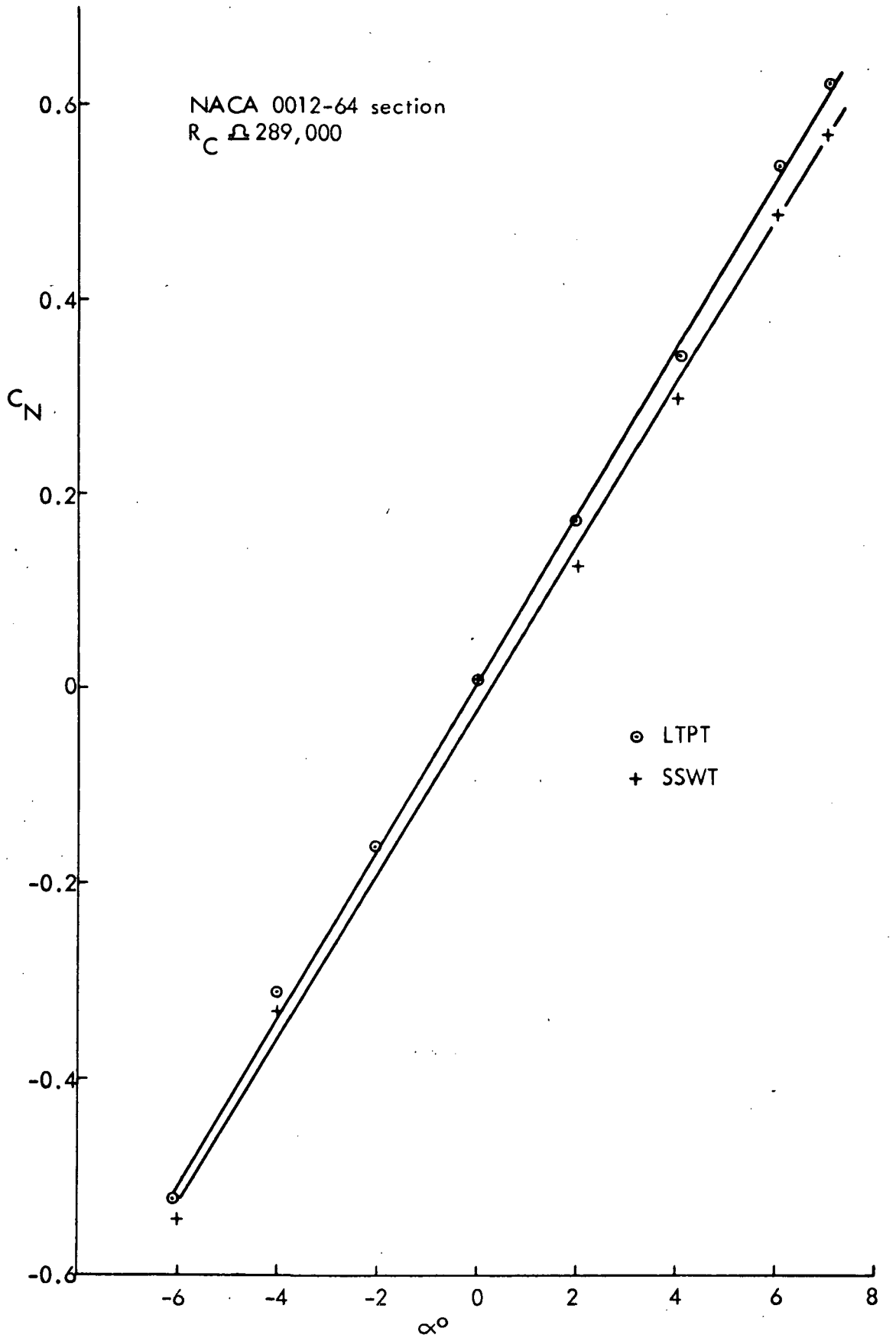

FIG. 2.4(a) C_N-α DATA FROM LTPT AND THE SELF STREAMLINING WIND TUNNEL.

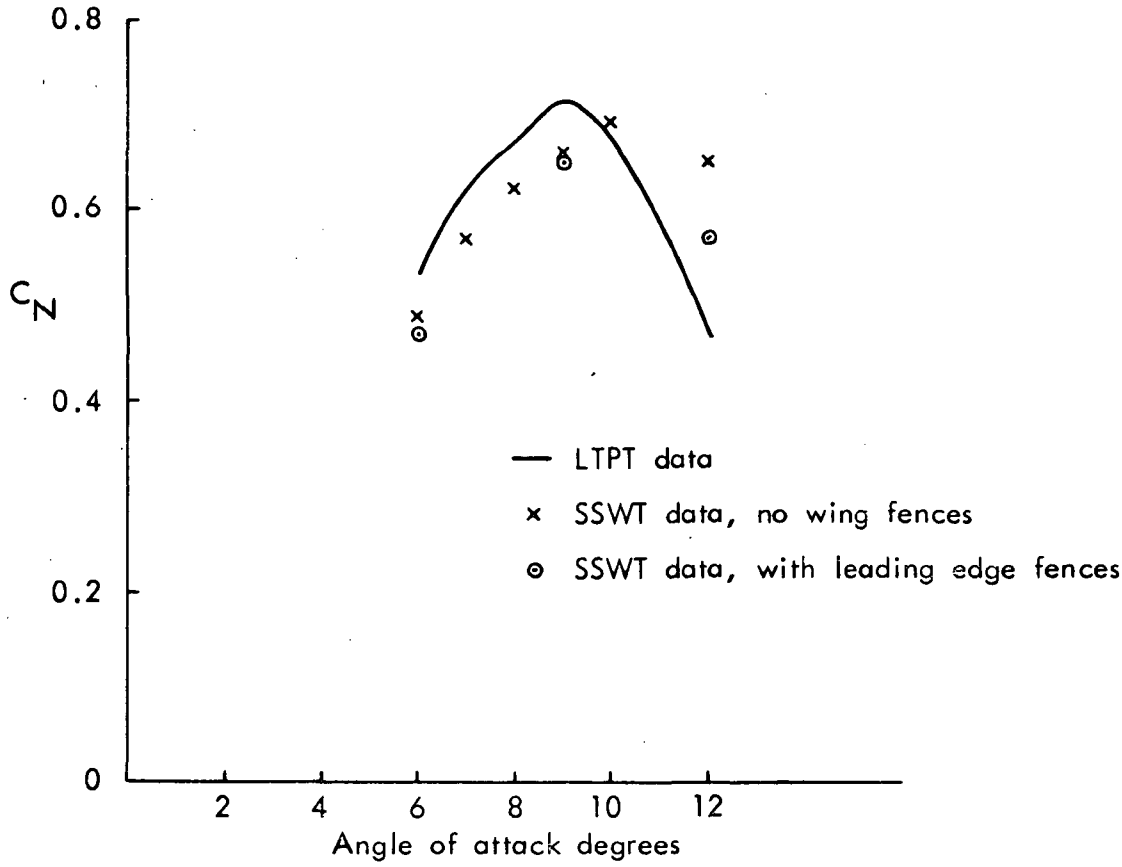

FIG 2.4(b) VARIATION OF C_N WITH ANGLE OF ATTACK IN STALL REGIME

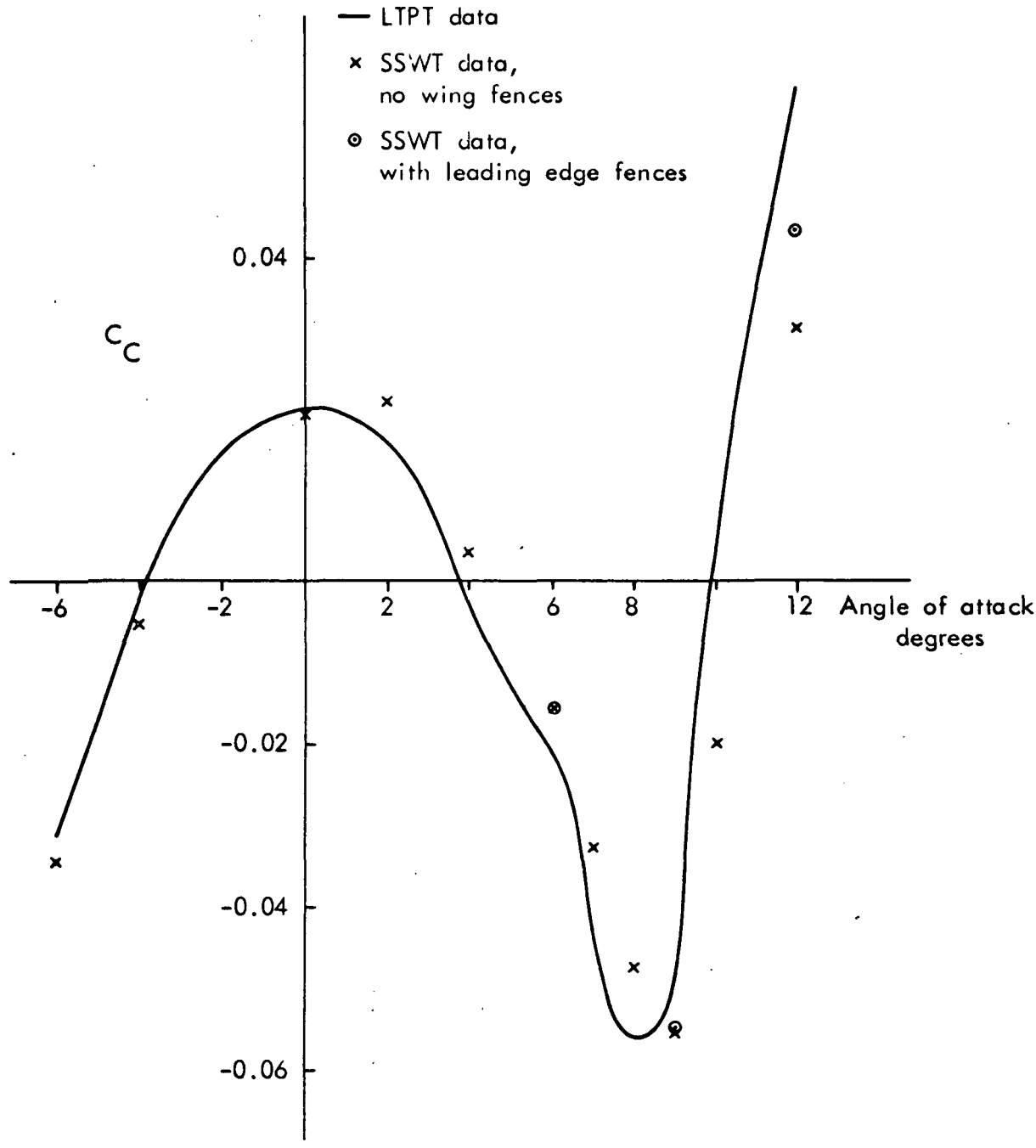

FIG 2.5 C_C - α DATA FROM LTPT AND SSWT

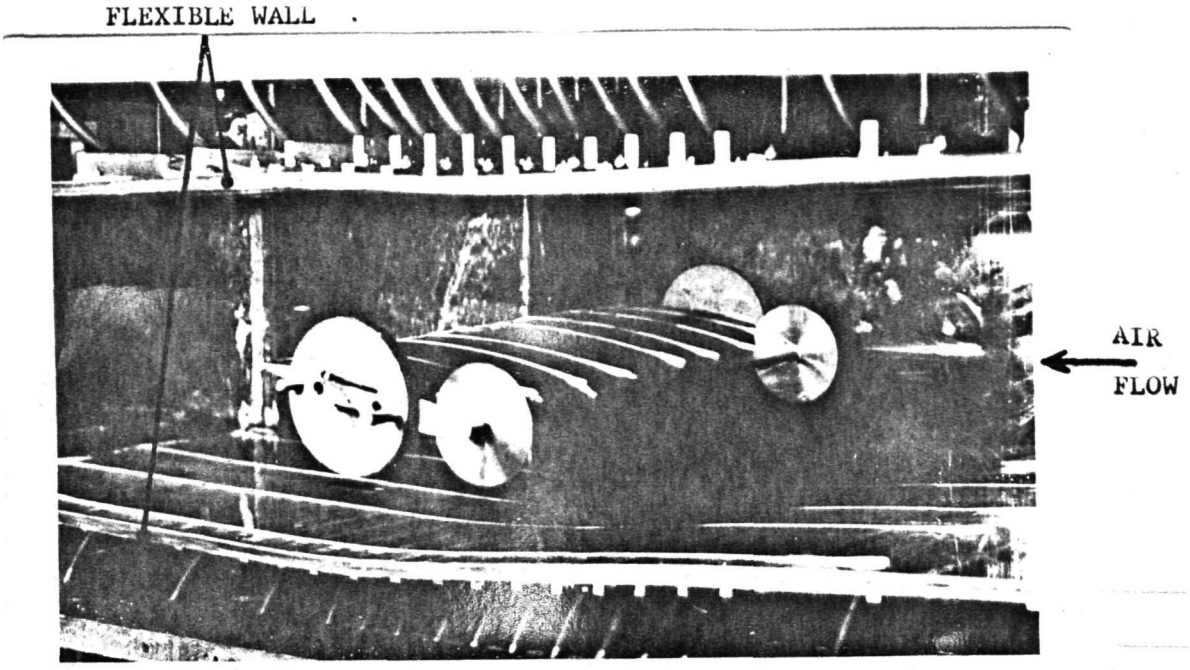

(a) General view of the low speed Self Streamlining Wind Tunnel, showing uniform flow on the pressure surface of the airfoil and on the bottom wall.

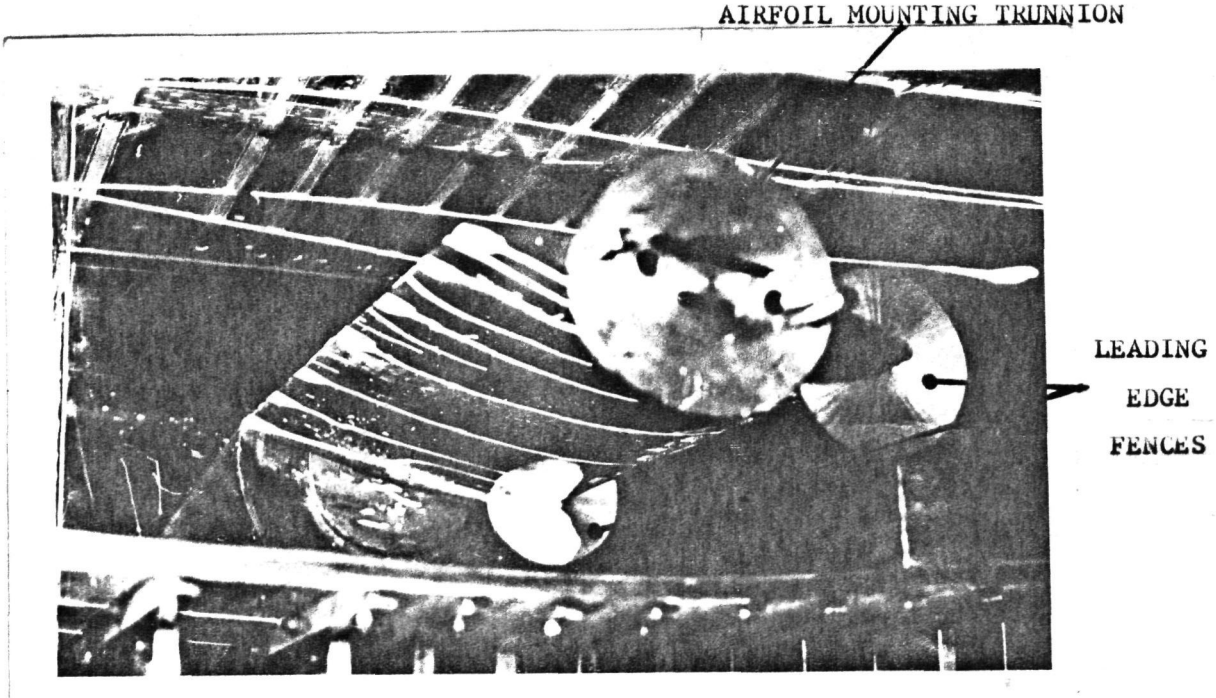

(b) View of the lower (suction) surface of the airfoil at $+12^{o}$ angle of attack, showing large reverse flow regions with three dimensional patterns.

FIG. 2.6 FLOW VISUALISATION ON THE AIRFOIL WITH LEADING EDGE FENCES FITTED.

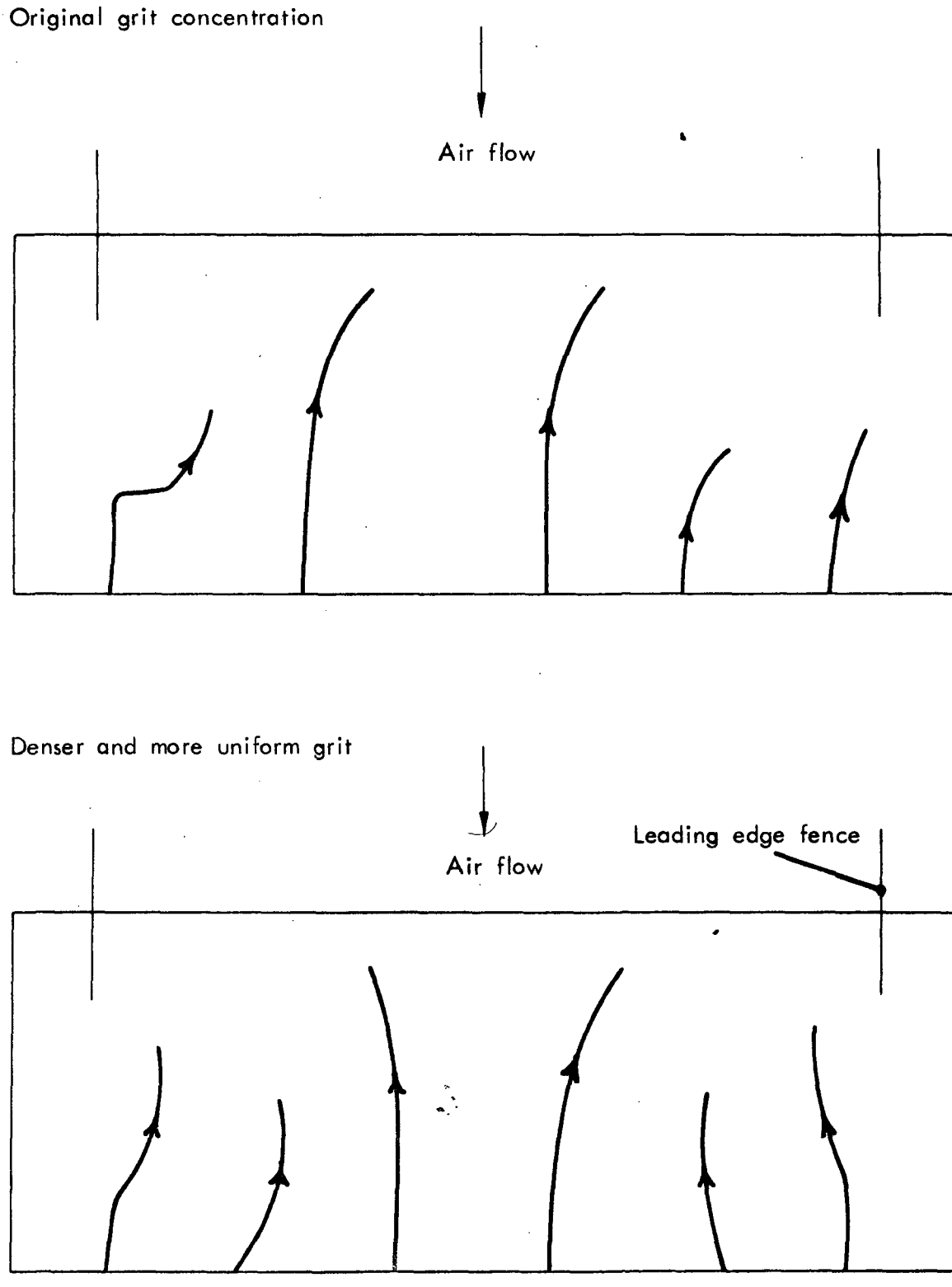

FIG 2.7 EFFECT OF LEADING EDGE GRIT CONCENTRATIONS ON SURFACE FLOW PATTERNS ON THE AIRFOIL.

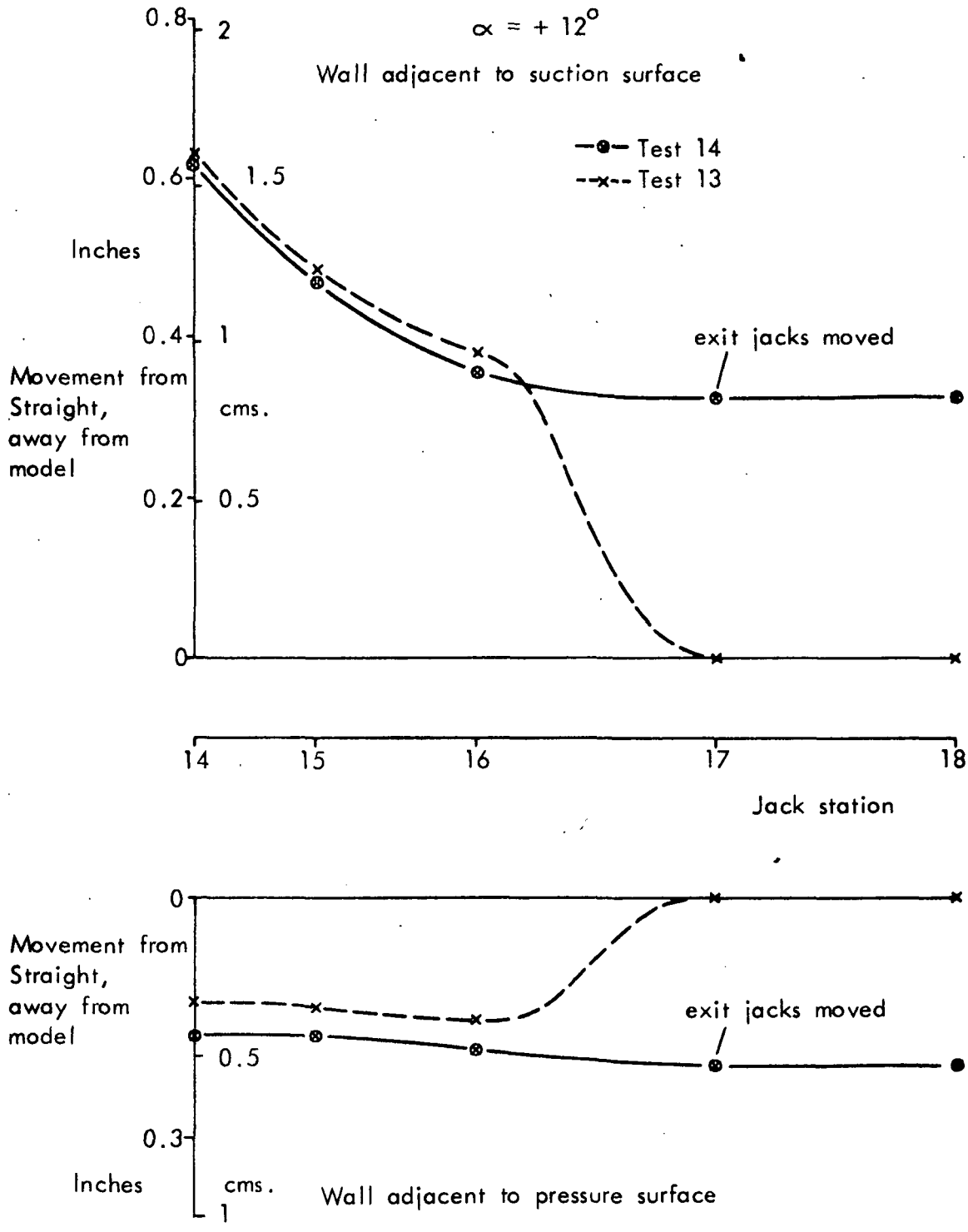

FIG. 2.8 FLEXIBLE-WALL CONTOURS WITH AND WITHOUT MOVEMENT OF THE EXIT JACKS.

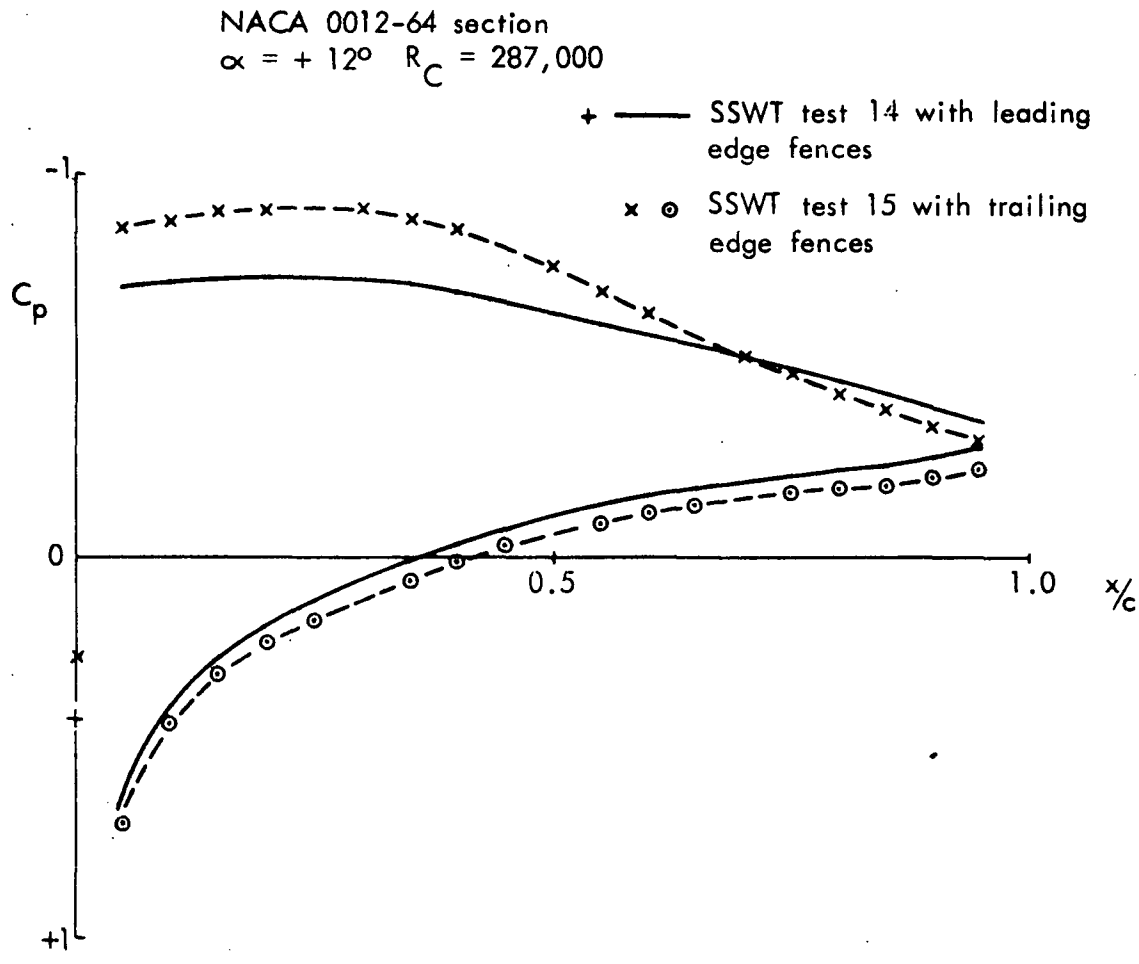

FIG. 2.9 EFFECT OF WING FENCES ON THE AIRFOIL PRESSURE DISTRIBUTION.

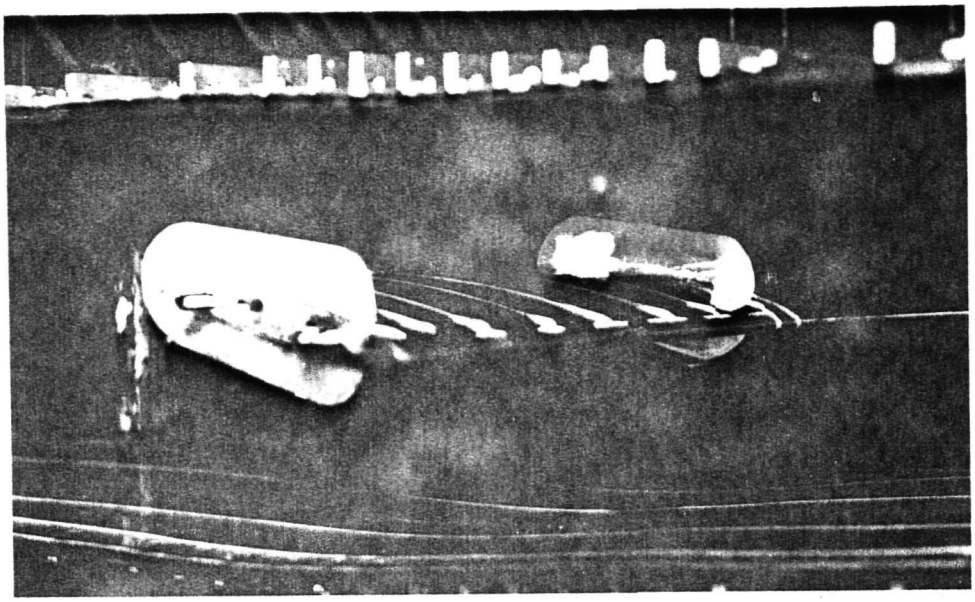

(a) Airfoil at +12^{o} angle of attack, trailing edge fences are fitted. The dye snows uniform flow over the upper (pressure) surface.

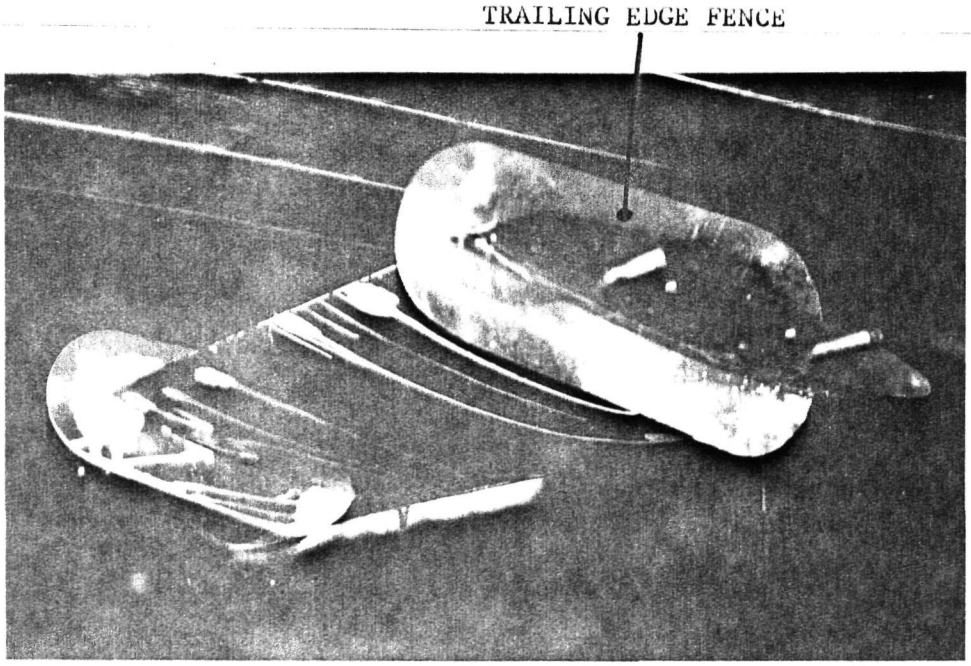

(b) Lower (suction) surface of the airfoil showing two dimensional reverse flow. Separation is indicated on the wing fences.

FIG. 2.10 FLOW VISUALISATION ON THE AIRFOIL WITH TRAILING EDGE FENCES FITTED.

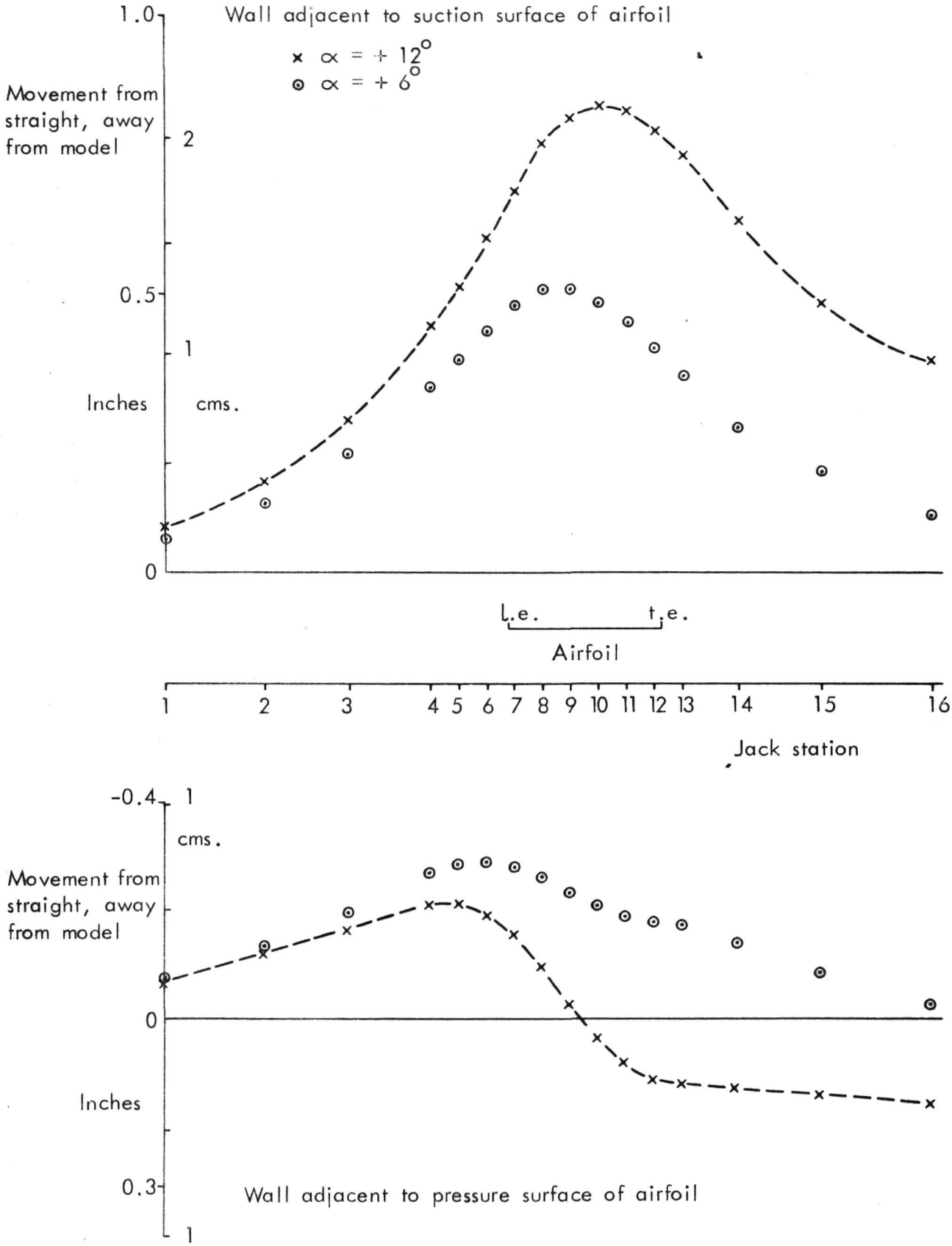

FIG. 2.11 TYPICAL FLEXIBLE-WALL CONTOURS

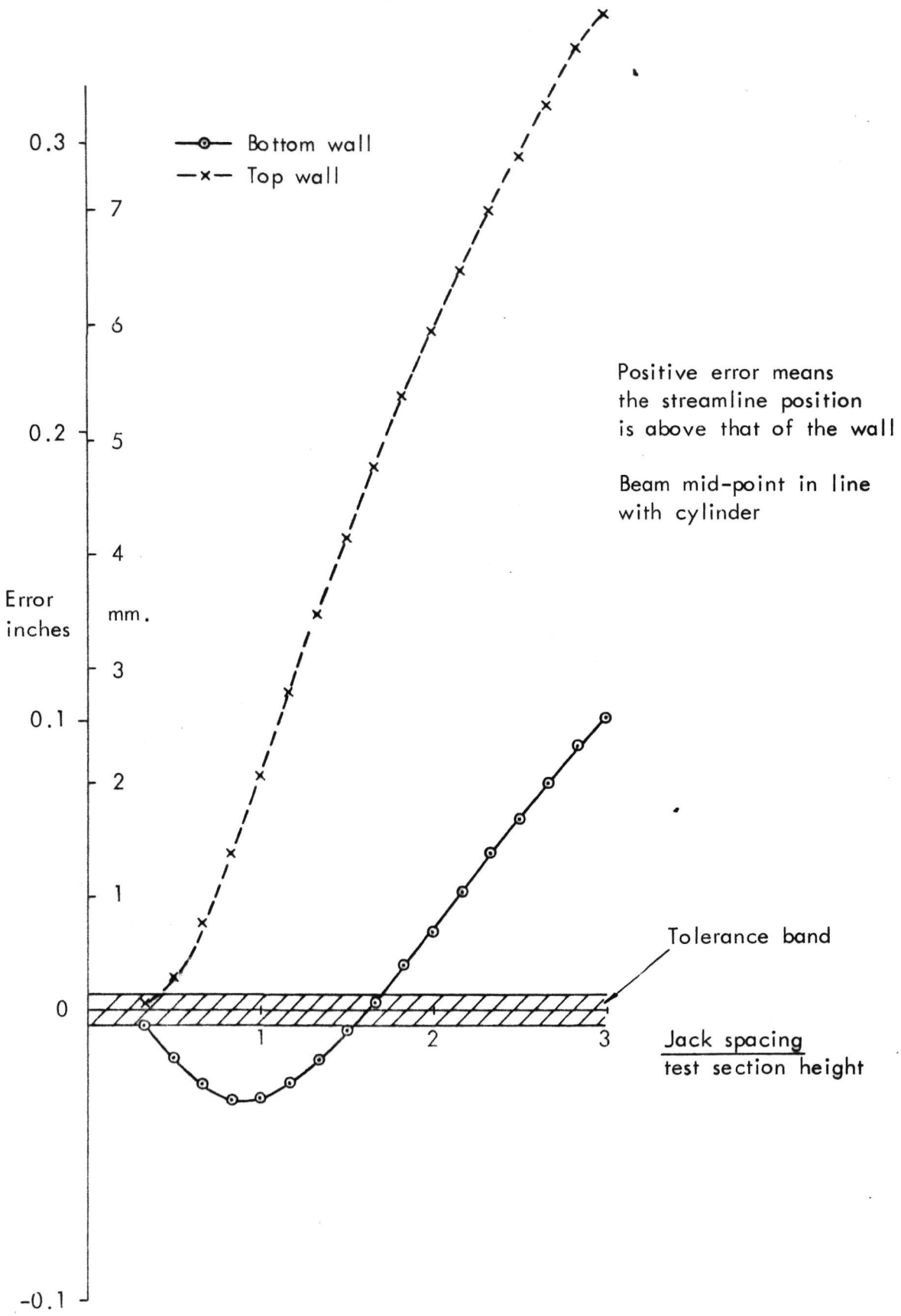

FIG. 4.1 BEAM AND STREAMLINE ANALYSIS

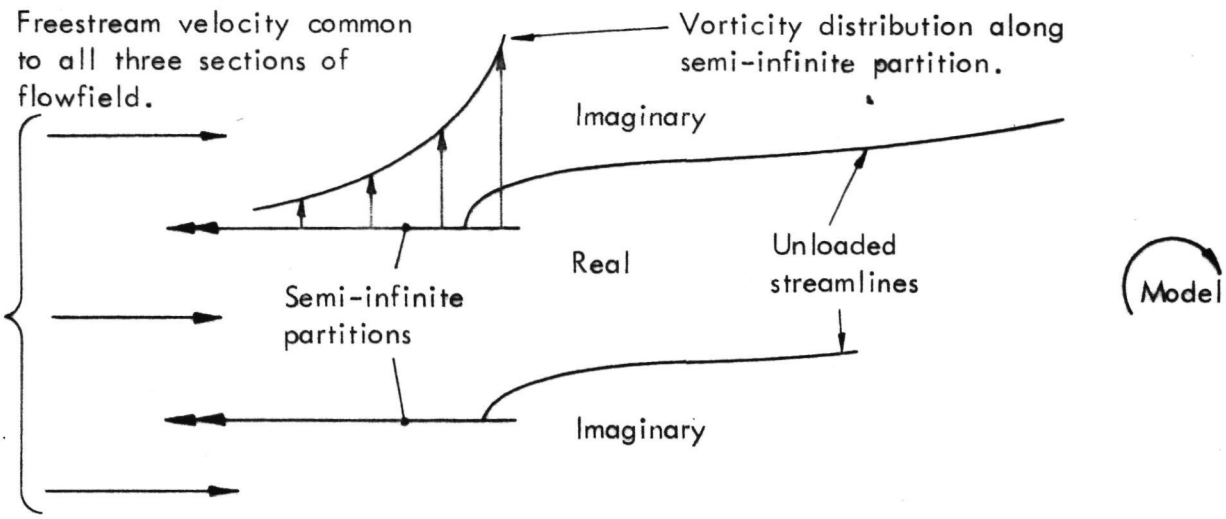

FIG. 4.2 An illustration of an analytical approximation to the flexible walled test section and lifting model. Only the upstream portion of test section is shown.

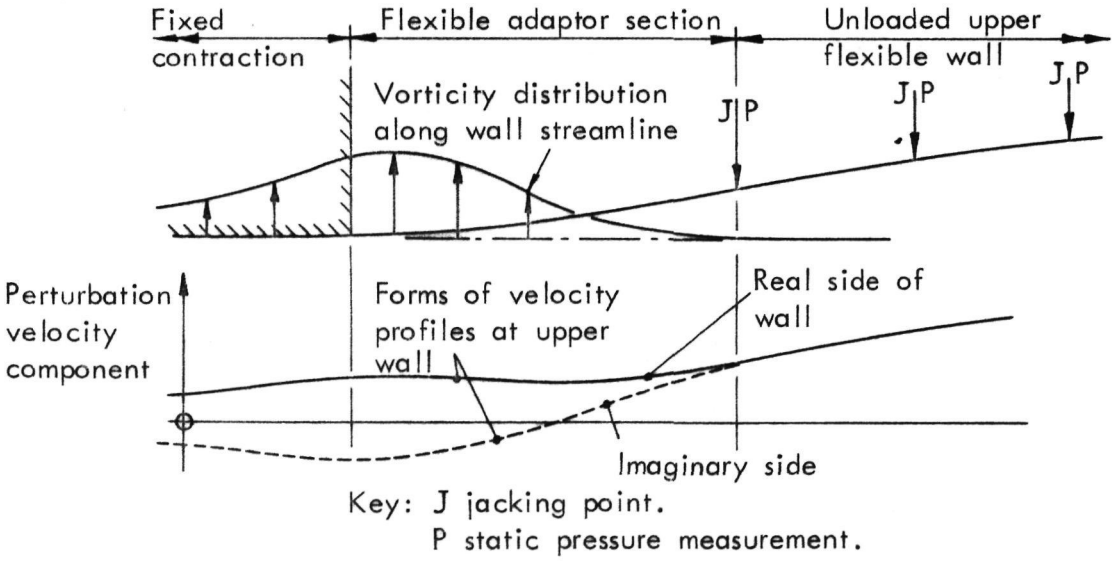

FIG 4.3 A closer approximation to the experimental arrangement in use at present. Details at the upstream upper wall.

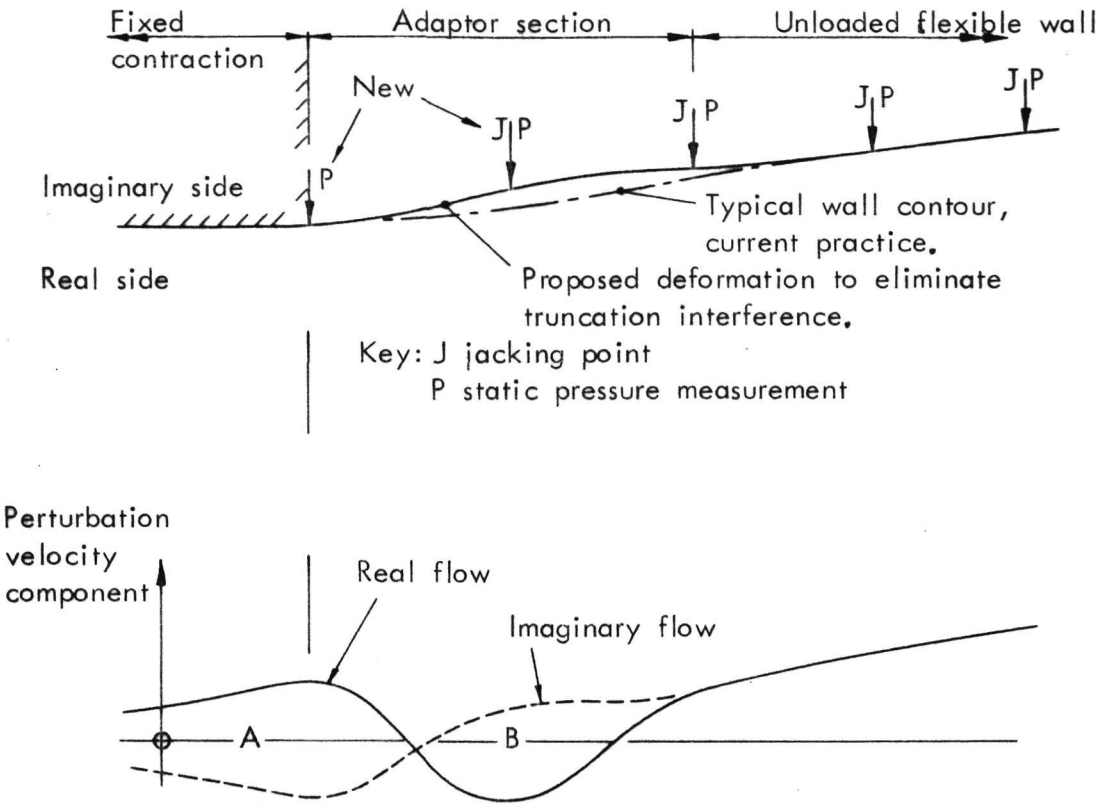

FIG. 4.4 The proposed deliberate deformation of an adaptor section inducing a local vorticity opposing that existing on a partition.

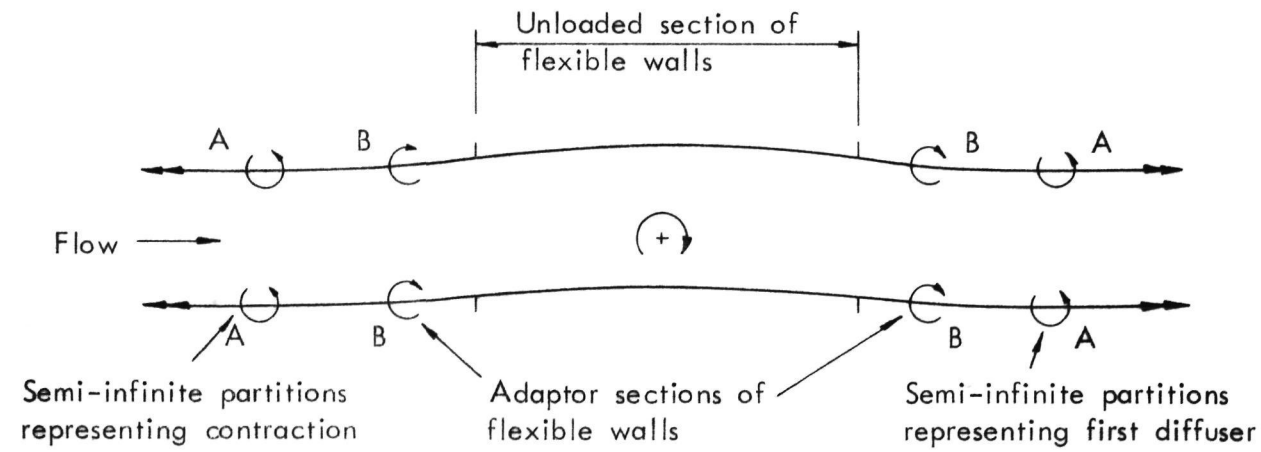

FIG. 4.5 *Symmetrical dispositions of vorticity at the ends of a test section,* eliminating the interference due to the effects of length truncation.

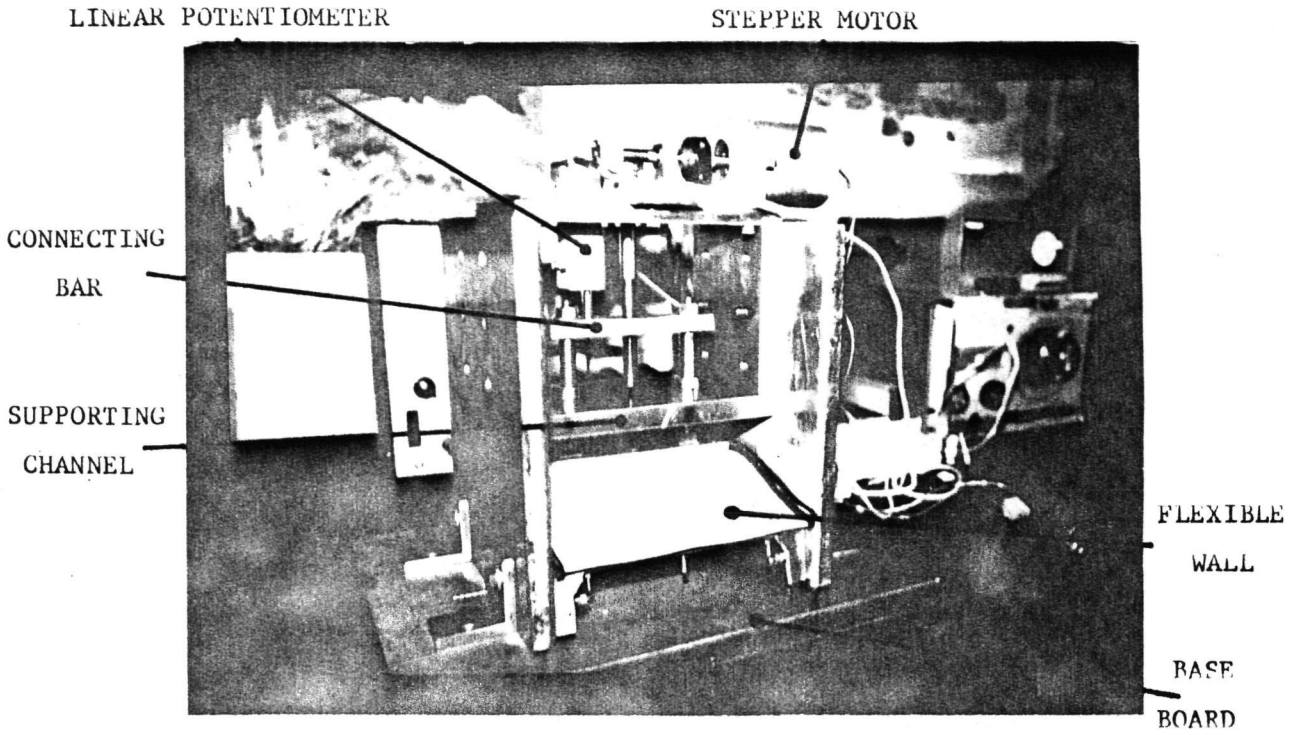

(a) Motorised jack at its highest position relative to adjacent fixed restraints on the flexible wall.

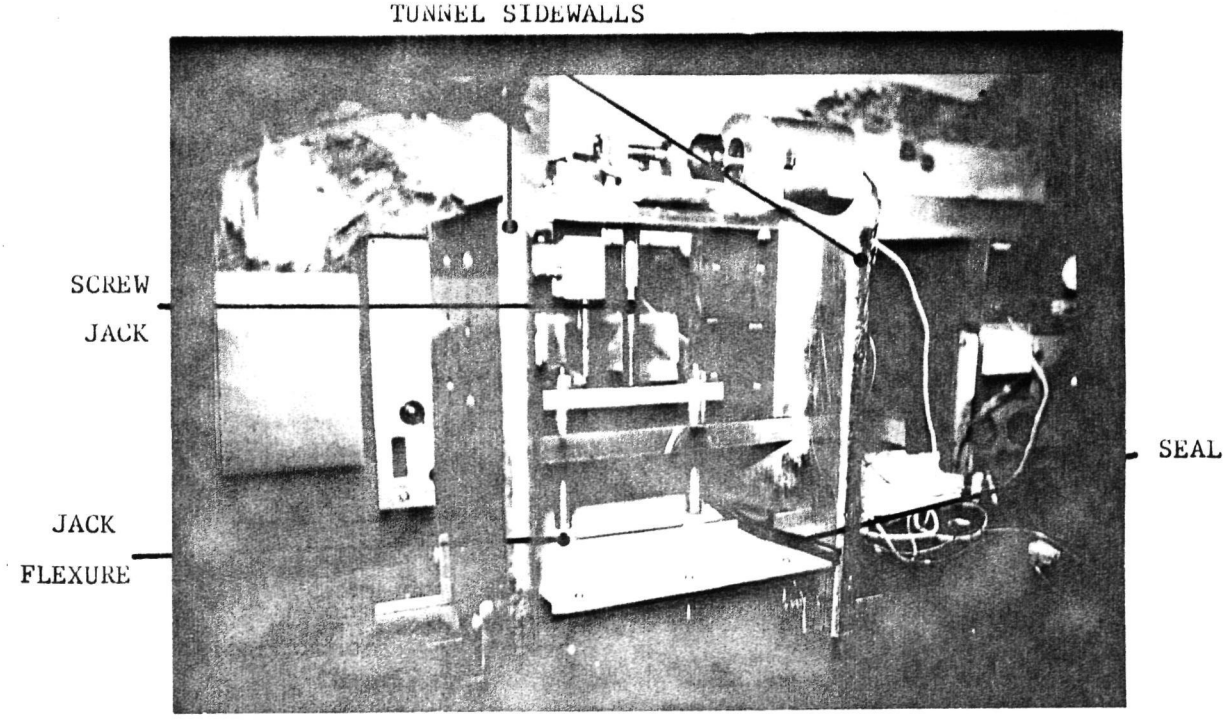

(b) Jack at its lowest position.

FIG. 5.1 . WALL JACK PROTOTYPE RIG.

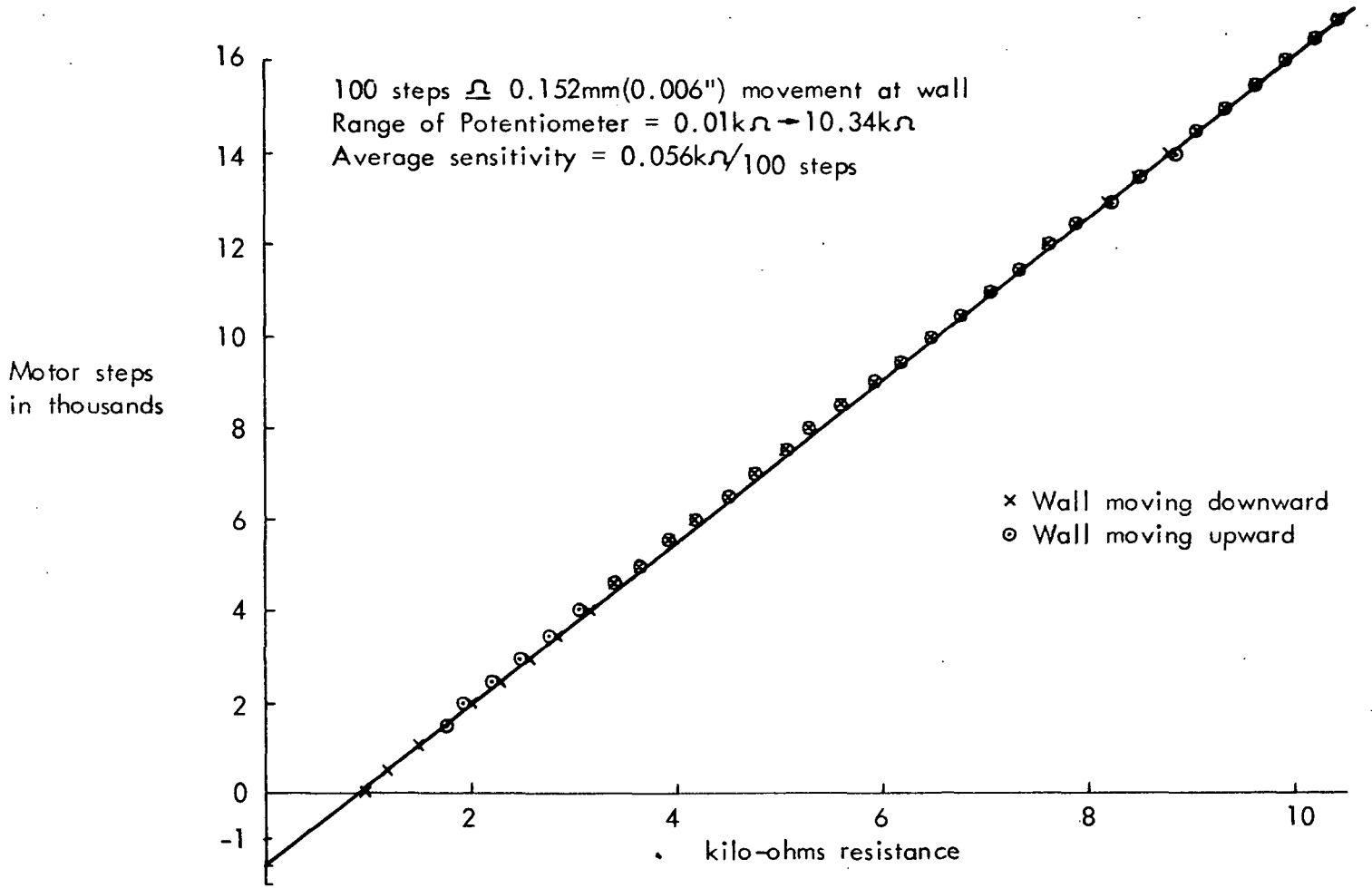

FIG. 5.2 LINEAR POTENTIOMETER CALIBRATION

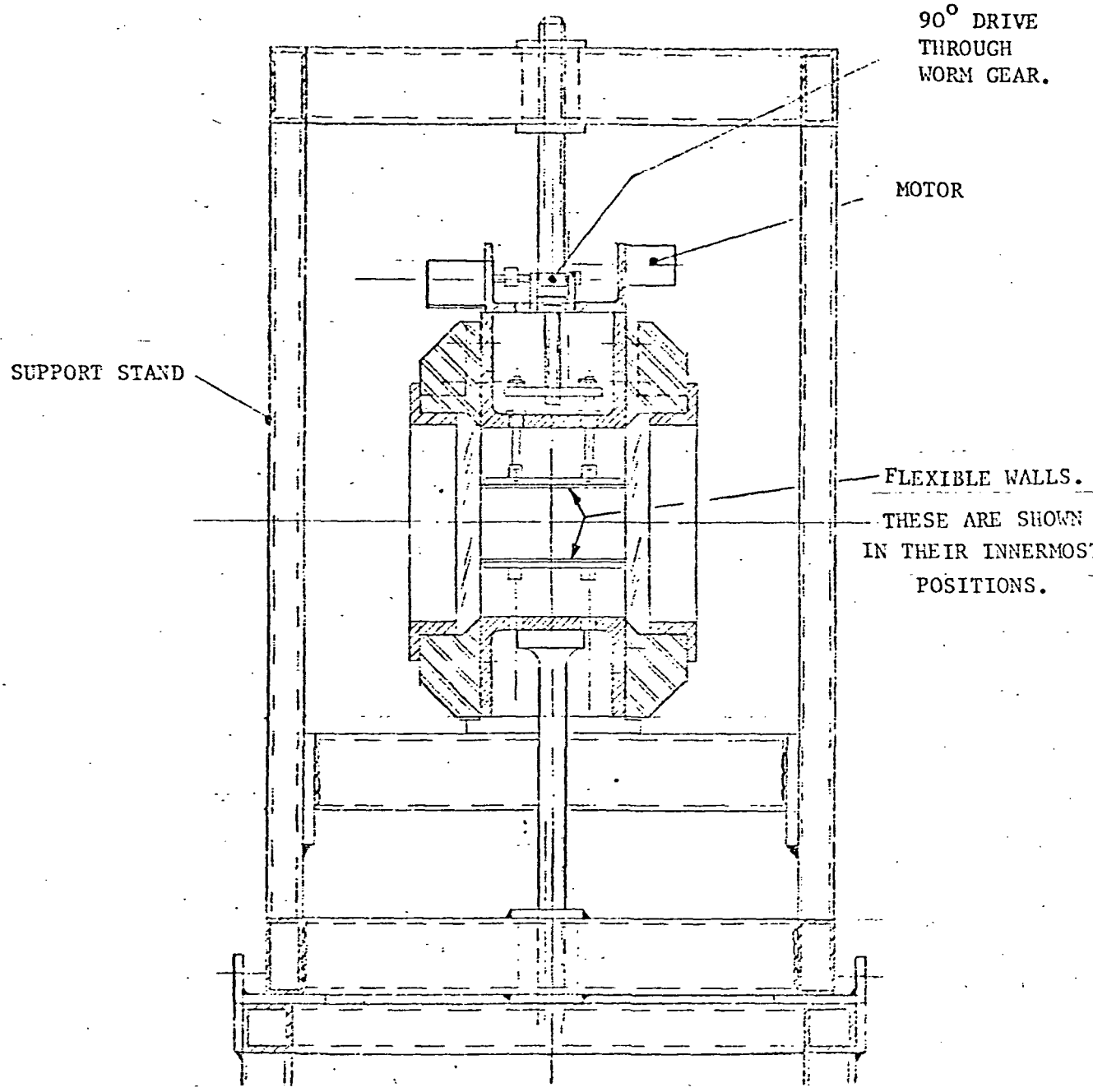

FIG. 5.3a TRANSONIC SELF-STREAMLINING TEST SECTION. VIEW DOWNSTREAM.

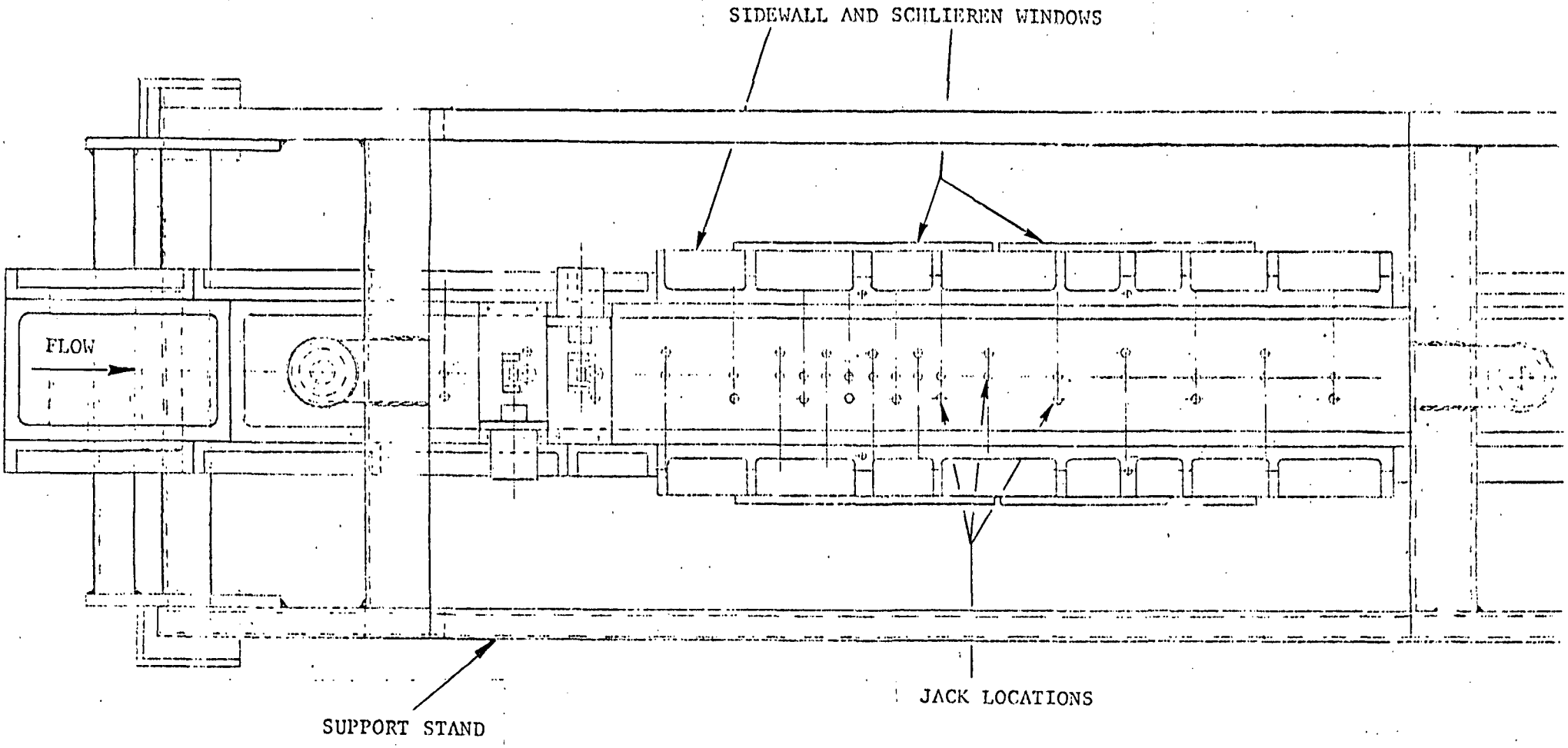

FIG. 5.3b TRANSONIC SELF-STREAMLINING TEST SECTION. PLAN VIEW.

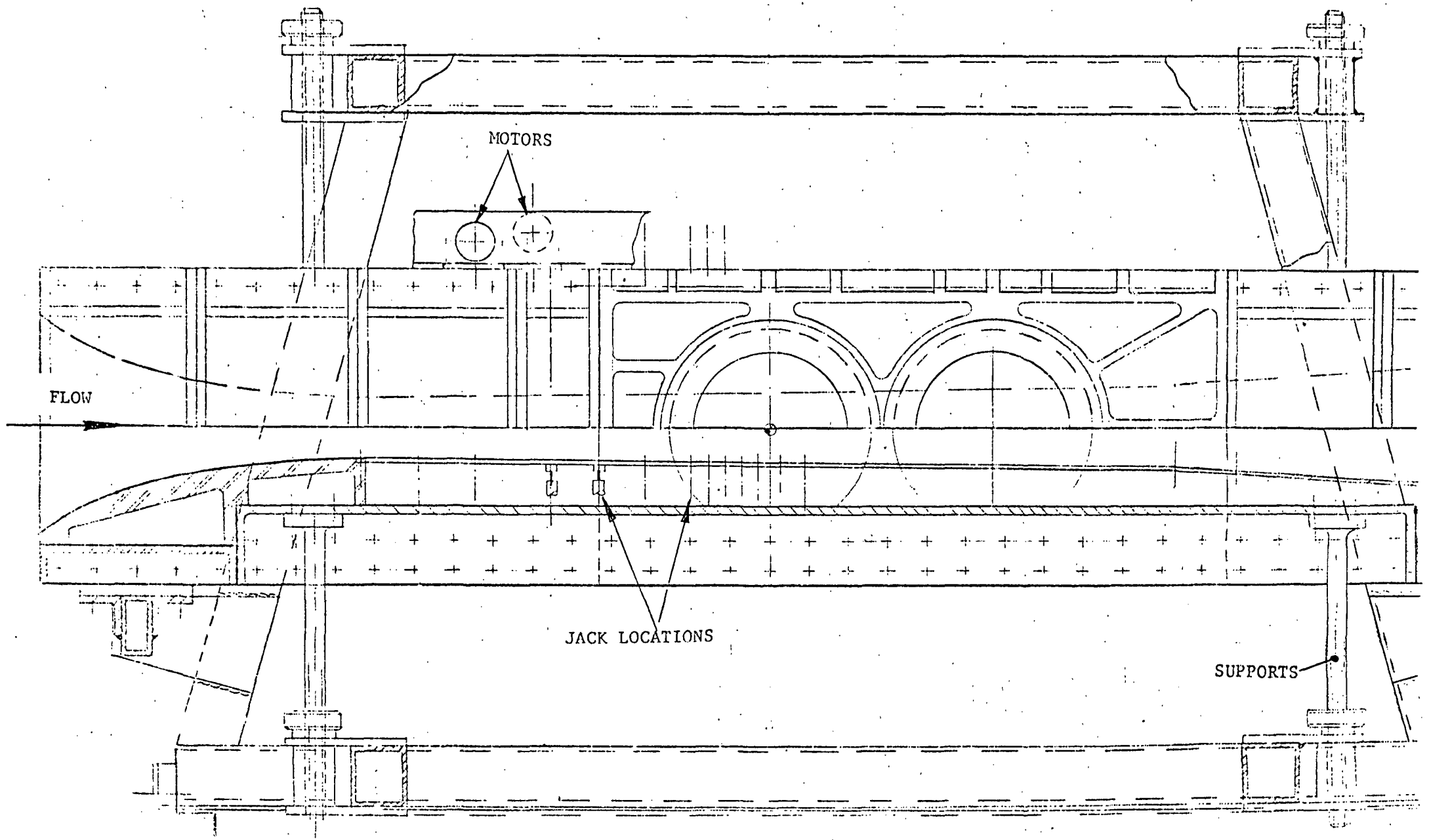

FIG. 5.3c TRANSONIC SELF-STREAMLINING TEST SECTION. SIDE ELEVATION.

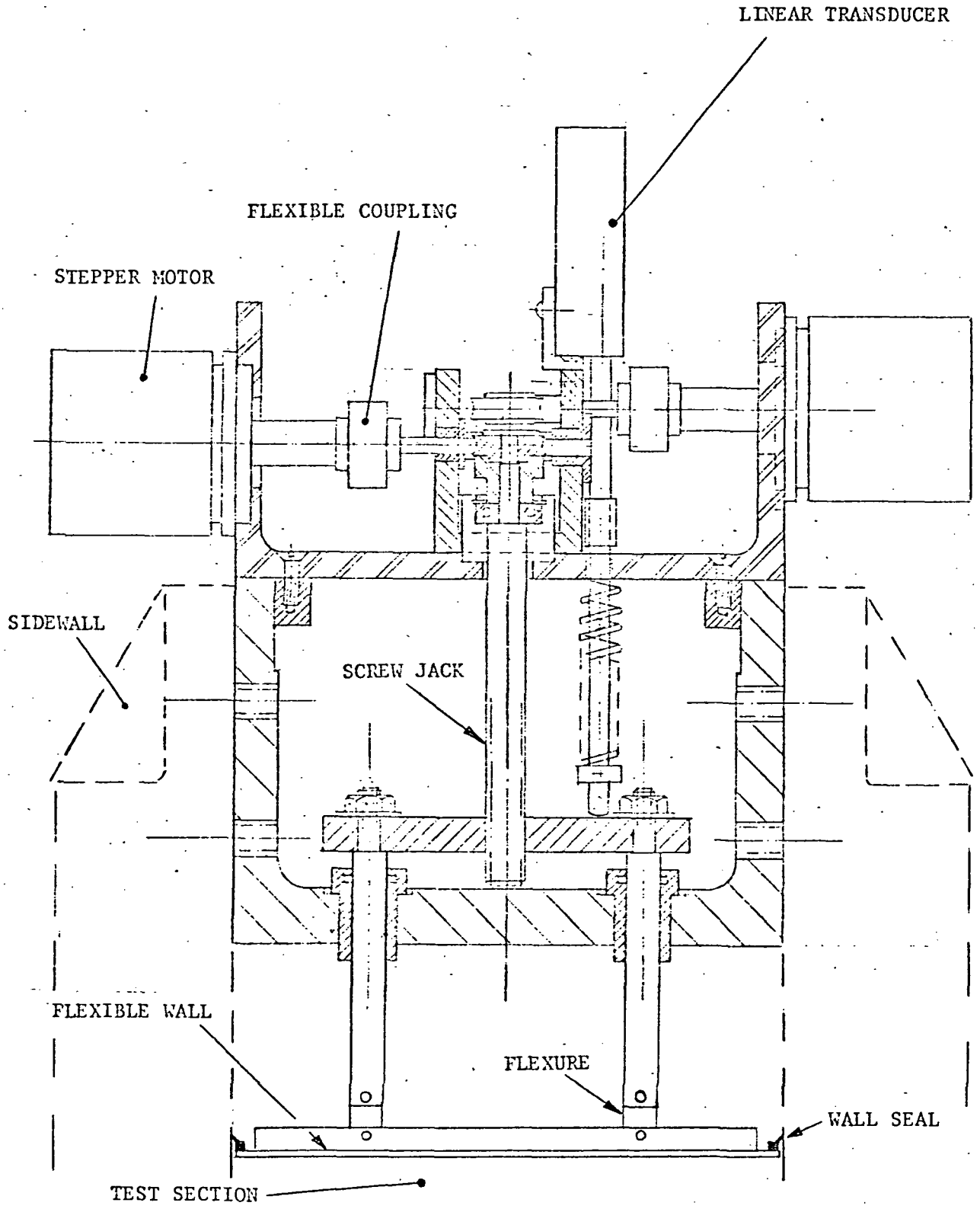

FIG. 5.3d TRANSONIC SELF-STREAMLINING TEST SECTION. DETAILS OF A JACKING POINT.